

Report #1

Greenop et al. have revised their manuscript substantially, improved the model tests and tailored it to show the consensus with previously published studies, rather than the focus on minor discrepancies of the original manuscript. I find this manuscript very much improved, but it still needs a few minor but important revisions. For the sake of simplicity, I will list these in chronological order, which is not necessarily the order of importance.

We thank the referee for the positive view on our revised manuscript and the improvements outlined below.

Line 175: spelling of name: Martínez-Botí

This has been changed.

Lines 192/238/248...: wuellerstorfi

This has been changed

Lines 205/208: Müller

This has been changed.

Lines 274 ff: what makes these “minor effects”? In particular the Miocene is a period of intense organic matter deposition (Monterey Formation!), that indicates systematic and substantial removal of isotopically light carbon from the ocean. Systematic changes in boundary conditions such as $\delta^{13}\text{C}$ -DIC and $p\text{CO}_2$ are not captured in the assumed constant uncertainty, which accounts only for random changes in boundary conditions. As such, these new $\delta^{11}\text{B}$ sw estimates are still not the ultimate answer, which is generally nicely acknowledged in this manuscript, but should be repeated in the conclusions (see comment below).

In the section here we refer to dissolution of calcium carbonate shells as a minor effect on the timescales we are concerned with as the CCD record of Palike et al. (2012) suggests there has not been substantial changes through time in this parameter. While the carbon isotopic composition of the whole ocean may have change, this was most likely accompanied by a pH change, and based on the modeling we present, the $\delta^{13}\text{C}$ -pH relationship has not changed significantly within the uncertainty bounds we use. We will reiterate the drawbacks to our methodology in the conclusion section as suggested below.

Line 460: its changes

This has been changed.

Lines 474/475: what is the “plausible” range and why? Please define “plausible”.

See response to reviewer 2. This has now been expanded on at the end of the section (lines 370-374).

Lines 584-587: the pH decrease may be at odds with the pCO₂ estimates shown in Beerling & Royer (2011), but more estimates have since been published that support the greater pCO₂ reconstructed from stomata (as already shown in Beerling & Royer). For instance, Zhang et al. (2013) show Miocene pCO₂ from alkenones >400 μatm, Bolton et al. (2016) went a step further and considering calcification changes in coccolithophores, they suggest Miocene pCO₂ may have been at least 50% higher compared to the Plio-Pleistocene. Foster et al. (2012) and Greenop et al. (2014) also suggest Miocene pCO₂ ~ 400 μatm, although they used an exceedingly low alkalinity of 1292 μmol/kg to yield these estimates, a value that is even more extreme than the alkalinity inventories tested in Fig. 7 (~1800-2600, considering that modern alk is somewhere around 2200 μmol/kg), which are considered “extreme and inconsistent with geological evidence” (Line 1138). Using more reasonable alkalinity values of ~2000 μmol/kg (Ridgwell 2005, Tyrrell & Zeebe 2004), the Miocene boron isotope pCO₂ estimates range closer to 500-600 μatm, clearly consistent with global evidence for warmer temperatures, and acidification as implied by models. There is uncertainty in all of these pCO₂ estimates but growing evidence for higher Miocene pCO₂ should be acknowledged and the argument that “proxy CO₂ and surface water pH estimates are not well described by the linear change in pH” should be revised in the light of this growing proxy data evidence. We agree with the reviewer that there is now good evidence for high CO₂ during the middle Miocene climatic optimum. We would question, however, the evidence that the early Miocene (17-23 Ma) has higher CO₂ than the Miocene climatic optimum (15-17 Ma; as would be suggested by a linear change in pH). There is currently a lack of CO₂ data for the early Miocene and consequently we will change the wording of the sentence to “proxy CO₂ and surface water pH estimates may not be well described by the linear change in pH” to reflect this uncertainty.

Line 704: please augment this sentence to “Despite some disagreements, and different uncertainties associated with each approach, the fact that...”.

This is just to reiterate that Greenop’s approach, like all others, has large

uncertainties as well, albeit due to different factors.

[This has been done.](#)

Line 712: controls

[This has been done.](#)

Line 1109: please specify where the “modern ocean” data are coming from, i.e. they are globally distributed and exceed the data shown in the Atlantic profiles. The reference to Foster et al. (2012) is not sufficient.

[The data are from all the ocean basins spanning the latitudes of 40N to 40S. This detail has been added to the figure caption.](#)

Line 1117: Please clarify that the error bars with 95% confidence due to external reproducibility only apply to the new data by Greenop et al. (this study), but not to Raitzch & Hönisch (2013), where they represent propagated uncertainties of external reproducibilities of time equivalent benthic foraminifer samples from different core sites in different ocean basins.

[This has been done.](#)

Line 1122: the color choice for the planktic foraminifera symbols is unfortunate and should be changed - the orange and red colors are nearly indistinguishable.

[This has been changed.](#)

Figure 8 caption: Please explain the 0.201 line

[This has been done.](#)

Figures 2 and 11: The $\delta^{11}\text{Bsw}$ data of Raitzsch & Hönisch (2013) are not plotted correctly, the data are all lower than originally presented, and so are the polynomial fits. The polynomial fits should probably be replaced by something like a 5-point running mean anyway, but I am puzzled why the data are lower than presented in the original study? This is particularly striking in Fig. 11, where the data are shifted even lower than in Fig. 2, below the 39.61‰ modern seawater $\delta^{11}\text{Bsw}$ estimate that the caption claims the data have been adjusted to (Lines 1175/1176). This must be rectified.

The original publication presented the data originating at a modern $\delta^{11}\text{Bsw}$ average of 39.6‰, so no adjustment of the original is necessary or justified.

[The polynomial fits have now been replaced by a 5-pt running average. The](#)

data were erroneously adjusted to 39.61‰ based on a single value for modern $\delta^{11}\text{B}_{\text{sw}}$ rather than an average of the two data points at 0 Ma in the Raitzsch & Hönisch (2013) dataset. We thank the reviewer for pointing this out and now no adjustment has now been made the $\delta^{11}\text{B}_{\text{sw}}$ data. There was also an error in the original dataset provided by the author of the study.

Report #2 Submitted on 18 Nov 2016

This study presents a new boron isotope curve of the Neogene based on foraminifera. The authors make the point that the $\delta^{11}\text{B}$ of forams is not an unfractionated archive for seawater, but is instead pH dependent, and therefore must be corrected using modelled ocean pH. The study goes into some depth on this modelling, and the assumptions made, and the results broadly agree with several other studies, although this study has considerably more data. Interestingly, the $\delta^{11}\text{B}$ seawater data also co-vary with records from other isotopic systems like Li, Mg and Ca.

Overall this is a well-written manuscript, with a detailed discussion on modelling, and some interesting outcomes in terms of seawater records, and I recommend it be published after some minor amendments listed below.

We thank the referee for taking the time to review our manuscript and the insightful comments outlined below.

Line 61: isn't carbonate weathering also a B source? Presumably they must be if carbonates are a major sink.

Carbonate weathering is also a source of boron to the ocean, however, in the river systems currently studied (Rose et al., 2000; Lemarchand and Gaillardet 2006) the weathering of silicate rocks dominates the riverine signal. The text has been updated to reflect this.

Line 63: is this low or high temperature ocean crust alteration?

Low temperature alteration. This has been updated in the text.

Line 116/Fig 3c: I would draw this as a line, rather than a series of data points, to make reading the graph easier.

This has been done.

Lines 11-125: for the non-B person, explain how this is not affected by CCD changes and associated pH changes?

This section refers to the $\delta^{13}\text{C}$ -pH gradient between the surface and thermocline depth so won't be affected by CCD change. The surface-to-deep gradient may be affected and this is something that is explored in the CYCLOPS modeling. When the CCD depth is changed within the bounds set out by Palike et al. (2012) we find the $\delta^{13}\text{C}$ -pH relationship does not vary outside the assigned uncertainty.

Line 145: referencing a manuscript in preparation is a little odd. Instead of referring to a manuscript in prep, we will describe the paper as “a follow up study by *Sosdian et al.*”.

Line 147: “nano” rather than “nanno”
This has been corrected.

Lines 154-161: what secondary standards were measured to ensure precision/accuracy? What is the precision of the $\delta^{11}\text{B}$ measurements?
The secondary standard used to ensure precision/accuracy is the Japanese Geological Survey *Porites* coral standard JCP. The details of this standard and the precision of the $\delta^{11}\text{B}$ measurements are outlined in section 2.5: Assessing uncertainty.

Section 2.4 and 2.5: you've listed all the parameters you used, but it would also be useful if you explained why you selected those parameters for the models.

These parameters were used to exceed any plausible changes within the Cenozoic. This is stated on lines 331-332, and is now, for improved clarity, reiterated at the end of section 2.4.

Line 513: explain this 0.1‰/Myr a bit more, especially given rapid Neogene weathering (and therefore input) changes.

The rate at which the $\delta^{11}\text{B}_{\text{sw}}$ can change is limited by the size of the oceanic boron reservoir compared the magnitude of the inputs and outputs. Therefore, even in the case of a large change in the weathering input, the residence time of boron in the ocean will exert a strong control on the rate at which $\delta^{11}\text{B}_{\text{sw}}$ can change. This has now been emphasized in the text.

Line 634: you say there are two controls on Mg, but then list three...
This has been changed.

Line 674-680: if you want to be inclusive about all the Li hypotheses, there

are also modelling papers on the Cenozoic: Li and West 2014, Wanner et al., 2014, Vigier and Godderis, 2015.

These references have been added to the appropriate sections. Thank you for this comment.

Line 671-698: this could be considered a bit oversimplified, given controls by carbonate and dolomite formation on Ca and Mg isotopes, and in turn their link with enhanced cation supply through weathering, and also potential temperature controls on dolomite formation. Also, Li is only affected by silicate weathering, whereas Ca and Mg are not – and Sr isotopes tell us that the Himalayas are dominantly (metamorphosed) carbonates. However, I agree that the cross-plots are compelling – but I think probably worth backing off a bit from the statements that it's only rivers, given, for example, that it's very hard to actually model Li by just invoking rivers (see Li and West 2014).

The final statement of this paragraph has been changed to be more inclusive of other factors that could control the Neogene major ion composition.

It's also interesting that there is an order of magnitude difference in residence time of the different elements – perhaps something worth mentioning and discussing. Why, for example, does the correlation between Li and B seem best, given the widest residence time difference?

This is a very interesting point. Here (and in the text) we hypothesize that the correlation between B and Li is best because the processes controlling the fluxes into and out of the ocean are similar. A more sophisticated approach would no doubt be necessary to fully unpick the trends we highlight here, but this is beyond the scope of this current manuscript but is something we will be following up on in due course.

In terms of the Ca record, I would take a look at Fantle and Tipper 2014 – especially their compilation of Neogene Ca isotopes (and their corrigendum to that graph), which suggests that the Griffith data are offset from others.

Many thanks for pointing us towards the Fantle and Tipper corrigendum. Here we chose to use the marine barite record of Griffith et al., 2008 as it is the archive that is the most likely to be a passive trace of Ca isotopes (Fantle, 2010). However, we acknowledge that the extent to which this is the case is still unknown and will make the distinction that the calcium isotopic composition of seawater is based on the marine barites.

P. Pogge von Strandmann, UCL, UK

A record of Neogene seawater $\delta^{11}\text{B}$ reconstructed from paired $\delta^{11}\text{B}$ analyses on benthic and planktic foraminifera.

Greenop Rosanna^{1,2*}, Hain, Mathis P.¹, Sosdian, Sindia M.³, Oliver, Kevin I.C.¹, Goodwin, Philip¹, Chalk, Thomas B.^{1,4}, Lear, Caroline H.³, Wilson, Paul A.¹, Foster, Gavin L.¹,

*Corresponding author

¹ Ocean and Earth Science, National Oceanography Centre Southampton, University of Southampton, Waterfront Campus, European Way, Southampton SO14 3ZH, UK

² School of Geography & Geosciences, Irvine Building, University of St Andrews, North Street, St Andrews, KY16 9AL, UK

³ School of Earth & Ocean Sciences, Cardiff University, Cardiff, CF10 3AT, UK

⁴ Department of Physical Oceanography, Woods Hole Oceanographic Institution, Woods Hole, Massachusetts, USA

Abstract:

The boron isotope composition ($\delta^{11}\text{B}$) of foraminiferal calcite, which reflects seawater pH, is a well-established proxy for reconstructing past seawater carbonate chemistry and, in the case of planktic foraminifera, past atmospheric CO_2 . However, to translate $\delta^{11}\text{B}$ measurements determined in calcareous fossils into pH we need to know the boron [isotopic](#) composition of the seawater in which they grew ($\delta^{11}\text{B}_{\text{sw}}$).

While a number of $\delta^{11}\text{B}_{\text{sw}}$ reconstructions exist, more work is needed to build confidence in our knowledge of this important parameter. Here we present a new Neogene $\delta^{11}\text{B}_{\text{sw}}$ record based on the $\delta^{11}\text{B}$ difference between paired measurements of planktic and benthic foraminifera and an estimate of the coeval water column pH gradient derived from planktic/benthic $\delta^{13}\text{C}$ data. To underscore this approach we present extensive tests using the CYCLOPS and GENIE carbon cycle models to demonstrate that the planktic/benthic $\Delta\text{pH}/\Delta\delta^{13}\text{C}$ relationship is relatively insensitive to ocean and carbon cycle changes. In keeping with previously published records, our

r.greenop 1/12/2016 17:45

Deleted: isotope

reconstruction suggests that $\delta^{11}\text{B}_{\text{sw}}$ was $\sim 37.5\text{‰}$ during the early and middle Miocene and rapidly increased from ~ 12 to 5 Ma to reach a plateau near the modern value of 39.61‰ . A similar pattern of change is evident in the seawater composition of the Mg, Li and Ca stable isotope systems. Concurrent shifts in the seawater isotopic composition of all four of these elements during the late Miocene are suggestive of a common forcing mechanism. Based on the observed direction of change we hypothesise that an increase in secondary mineral formation during continental weathering may have affected the isotopic composition of the riverine input to the ocean since $\sim 12\text{-}15\text{ Ma}$.

1. Introduction

Key to determining the relationship between CO_2 and climate in the geological past is the calculation of reliable estimates of absolute CO_2 through time. In recent years the boron isotope composition ($\delta^{11}\text{B}$) of foraminiferal calcite has become a high-profile tool for reconstructing CO_2 beyond the last 800 kyrs and throughout the Cenozoic Era (Foster, 2008; Hönisch et al., 2009; Pearson et al., 2009; Bartoli et al., 2009; Foster et al., 2012; Badger et al., 2013; Henahan et al., 2013; Greenop et al., 2014; Martínez-Botí, et al., 2015a). Yet long-term change in the boron isotope composition of seawater ($\delta^{11}\text{B}_{\text{sw}}$) is currently poorly constrained and represents a major source of the uncertainty associated with $\delta^{11}\text{B}$ -determined CO_2 estimates (e.g. Pearson et al., 2009). In the modern ocean boron is a conservative element with a spatially invariant isotope ratio (39.61‰ ; Foster et al., 2010), but this value is subject to change through geological time. The residence time of boron in the ocean is estimated to lie between 11 and 17 Myrs (Lemarchand et al., 2000). Therefore we can expect the uncertainty associated with $\delta^{11}\text{B}_{\text{sw}}$ to be an important factor in CO_2 estimates beyond the late Pliocene ($\sim 4\text{-}5\text{ Ma}$, Palmer et al., 1998; Lemarchand et al., 2000; Pearson et al., 2009; Foster et al., 2012; [Anagnostou et al. 2016](#)).

The ocean boron budget and its isotopic composition are controlled by a number of inputs and outputs (Fig. 1). However, because the magnitude of the boron fluxes between land, the ocean and the atmosphere in the modern are still poorly understood, the residence time and changes in both concentration ($[\text{B}]_{\text{sw}}$) and isotopic composition ($\delta^{11}\text{B}_{\text{sw}}$) through time remain uncertain. The main inputs of B into the

ocean are silicate weathering, [and to a lesser extent evaporite and carbonate weathering](#), delivered to the ocean by rivers (Lemarchand et al., 2000; [Rose et al., 2000; Lemarchand and Gaillardet, 2006](#)), hydrothermal vents (You et al., 1993) and fluid expelled from accretionary prisms (Smith et al., 1995). The major loss terms are [low temperature](#) oceanic crust alteration (Smith et al., 1995), adsorption onto sediments (Spivack and Edmond, 1987) and co-precipitation into carbonates (Hemming and Hanson, 1992). In [the](#) case of all three outputs the light ^{10}B isotope is preferentially removed relative to ^{11}B , such that the seawater $^{11}\text{B}/^{10}\text{B}$ ratio ($\delta^{11}\text{B}_{\text{sw}}$, 39.61‰) is significantly greater than that of the cumulative inputs ($\delta^{11}\text{B}$ of ~10.4‰; Lemarchand et al., 2000). Our understanding of the modern boron fluxes outlined above, and illustrated in Fig. 1, implies a significant imbalance between inputs and outputs and consequently the poorly constrained ocean-atmosphere boron fluxes may also be an important part of the ocean's modern boron mass balance (Park and Schlesinger, 2002). [Here](#), however, we follow Lemarchand et al., (2000) [in assuming that](#) atmospheric fluxes are unlikely to have varied significantly on geological timescales and therefore will not be discussed further in reference to the Neogene $\delta^{11}\text{B}_{\text{sw}}$ record [we present](#).

Unlike many other isotopic systems (e.g. $\delta^7\text{Li}_{\text{sw}}$, $\delta^{26}\text{Mg}_{\text{sw}}$, $\delta^{44/40}\text{Ca}_{\text{sw}}$, $^{87}\text{Sr}/^{86}\text{Sr}$), to date, no [direct](#) archive has been [documented for](#) $\delta^{11}\text{B}_{\text{sw}}$. This is a result of the pH-dependent boron speciation in seawater upon which the $\delta^{11}\text{B}$ -pH proxy is based (Hemming & Hanson 1992) that imparts a pH dependency on the $\delta^{11}\text{B}$ of all marine precipitates so far examined. Empirical reconstructions of $\delta^{11}\text{B}_{\text{sw}}$ must therefore use “indirect” approaches. So far four approaches have been applied to the problem (Fig. 2): (1) geochemical modeling (Lemarchand et al., 2000), (2) $\delta^{11}\text{B}$ analysis of halites (Paris et al., 2010), (3) measurements of benthic foraminiferal $\delta^{11}\text{B}$ coupled to various assumptions about past changes in ocean pH (Raitzsch and Hönisch, 2013), and (4) measurements of $\delta^{11}\text{B}$ in surface and thermocline dwelling foraminifera coupled with additional information on the pH gradient of the surface ocean (Palmer et al., 1998; Pearson and Palmer 1999, Pearson and Palmer 2000; Anagnostou et al., 2016). Geochemical modelling of the changes in the flux of boron into and out of the ocean through time has been used to suggest that $\delta^{11}\text{B}_{\text{sw}}$ increased from 37‰ at 60 Ma to $40\text{‰} \pm 1\text{‰}$ today, driven by a combination of processes including changing boron continental discharge (Lemarchand et al., 2000). In the case of approach 2,

- r.greenop 4/12/2016 09:53
Deleted: In the context of this study
- r.greenop 4/12/2016 09:54
Deleted: and
- r.greenop 4/12/2016 09:54
Deleted: m
- r.greenop 4/12/2016 09:54
Deleted: e
- r.greenop 4/12/2016 09:55
Deleted: discovered that simply records unaltered
- r.greenop 1/12/2016 17:46
Deleted:

103 while modern natural halites reflect $\delta^{11}\text{B}_{\text{sw}}$ (39.7 ‰) with no apparent fractionation,
 104 measurement of $\delta^{11}\text{B}$ in ancient halites yield isotopic ratios that are significantly
 105 lower than all other approaches (Fig. 2; Paris et al., 2010), with implausible
 106 variability among samples of the same age (7‰ range), thereby casting doubt over
 107 the reliability of this approach (Raitzsch and Hönisch, 2013). In the case of approach
 108 3, $\delta^{11}\text{B}_{\text{sw}}$ is calculated from globally distributed benthic $\delta^{11}\text{B}$ data with an imposed
 109 degree of deep-ocean pH change (Fig. 2; Raitzsch and Hönisch, 2013). This method
 110 hinges on two key assumptions: (a) a near linear surface water pH increase of 0.39
 111 over the past 50 Myrs taken from the average pH output from a number of modeling
 112 studies (Berner and Kothavala, 2001; Tyrrell and Zeebe, 2004; Ridgwell, 2005), and
 113 (b) a prescribed constant surface-to-deep ocean pH gradient of 0.3 (Tyrrell and
 114 Zeebe, 2004, and modern observations). The modeled surface pH and estimated fixed
 115 pH gradient is then used to estimate deep ocean pH, and then convert benthic
 116 foraminiferal $\delta^{11}\text{B}$ measurements to $\delta^{11}\text{B}_{\text{sw}}$. This approach yields broadly similar
 117 results to geochemical modeling (Fig. 2). The fourth approach exploits the non-linear
 118 relationship between $\delta^{11}\text{B}$ and pH alongside estimated pH gradients in the ocean to
 119 constrain $\delta^{11}\text{B}_{\text{sw}}$ (Palmer et al., 1998; Pearson and Palmer 1999, Pearson and Palmer
 120 2000) and is the basis of the approach used in this study. The advantage of this
 121 method is that $\delta^{11}\text{B}_{\text{sw}}$ can be reconstructed empirically without relying on a priori
 122 absolute-pH constraints. The non-linear relationship between $\delta^{11}\text{B}$ and pH means that
 123 the pH difference between two $\delta^{11}\text{B}$ data points varies as a function of $\delta^{11}\text{B}_{\text{sw}}$ (Fig. 3).
 124 Consequently, if the size of the pH gradient can be estimated then there is only one
 125 $\delta^{11}\text{B}_{\text{sw}}$ value that is consistent with the foraminiferal $\delta^{11}\text{B}$ measurements and the
 126 specified pH gradient irrespective of the absolute pH (Fig. 3c). Previously this
 127 approach has been applied to pH variations in the surface ocean and used in studies
 128 of Cenozoic $p\text{CO}_2$ to account for changes in $\delta^{11}\text{B}_{\text{sw}}$ (determined using $\delta^{11}\text{B}$ in surface
 129 and thermocline-dwelling foraminifera) (Fig. 2) (Palmer et al., 1998; Pearson and
 130 Palmer 1999, Pearson and Palmer 2000; Anagnostou et al., 2016). This approach uses
 131 a constant pH gradient between the surface and some depth proximal to the oxygen
 132 minimum zone and the boron isotope values of a mixed layer dwelling species and
 133 thermocline dweller to calculate a value for $\delta^{11}\text{B}_{\text{sw}}$ (Pearson and Palmer, 1999). The
 134 resulting record suggests that $\delta^{11}\text{B}_{\text{sw}}$ varies between 37.7‰ and 39.4‰ through the
 135 Neogene (Fig. 2) (Pearson and Palmer, 2000).

r.greenop 1/12/2016 18:11

Deleted: intermediate

r.greenop 1/12/2016 18:13

Deleted: two

r.greenop 1/12/2016 18:13

Deleted: *dependent*

r.greenop 1/12/2016 18:13

Formatted: Font:Italic

139 | The same method, but using planktic-benthic instead of surface planktic-thermocline
 140 | planktic $\delta^{11}\text{B}$ gradients to calculate $\delta^{11}\text{B}_{\text{sw}}$, was recently applied to the middle
 141 | Miocene where it yielded a $\delta^{11}\text{B}_{\text{sw}}$ of $37.6^{+0.4}_{-0.5}$ ‰ (Foster et al., 2012). A further
 142 | modification to the method of Pearson and Palmer (1999) was also proposed in that
 143 | study wherein $\delta^{13}\text{C}$ in foraminiferal calcite was used to estimate the surface-to-deep
 144 | pH gradient (Foster et al., 2012). Here, we reconstruct $\delta^{11}\text{B}_{\text{sw}}$ for the last 23 Ma, the
 145 | Neogene, based on this modified approach. We undertake extensive sensitivity tests
 146 | using both the CYCLOPS carbon cycle box model and the GENIE Earth system
 147 | model to define the plausible range in the relationship between surface/deep pH
 148 | difference and $\delta^{13}\text{C}$ difference, which is an essential parameter for this approach.
 149 | Finally, we employ a Monte Carlo approach for comprehensive propagation of
 150 | uncertainty in all input parameters and we focus on reconstructing $\delta^{11}\text{B}_{\text{sw}}$ – the
 151 | implications of our work for understanding the evolution of Neogene ocean pH and
 152 | atmospheric $p\text{CO}_2$ will be documented elsewhere.

r.greenop 1/12/2016 18:14

Deleted:

r.greenop 1/12/2016 18:14

Deleted:

153 | 2. Methods

154 | 2.1 Site Locations and Age Models

155 | Foraminifera from four sites are used to construct the planktic-benthic $\delta^{11}\text{B}$ pairs;
 156 | Ocean Drilling Program, ODP, Site 758 and ODP Site 999 for the Pleistocene and
 157 | Pliocene samples and ODP Site 926 and Site 761 for the Miocene (Fig. 4) (this study;
 158 | Foster et al., 2012; Martínez-Botí et al., 2015a, [and a follow up study by](#) Sosdian et
 159 | al.). We also incorporate the middle Miocene planktic-benthic pair from Site 761 in
 160 | Foster et al. (2012). To place all data from all sites on a single age model we use the
 161 | nanno and planktic foraminifera stratigraphy from sites 999, 926 and 761 (Shipboard
 162 | Scientific Party, 1997; Shipboard Scientific Party, 1995; Zeeden et al., 2013;
 163 | Holbourn et al., 2004) updated to GTS2012 (Gradstein et al., 2012). At Site 758 the
 164 | magnetostratigraphy (Shipboard Scientific Party, 1989) is used and updated to
 165 | GTS2012 (Gradstein et al., 2012).

r.greenop 1/12/2016 17:40

Deleted: in prep

2.2 Boron Isotope Analysis and pH Calculation

The boron isotope measurements (expressed in delta notation as $\delta^{11}\text{B}$ – permil variation) were made relative to the boric acid standard SRM 951; (Catanzaro et al., 1970). Boron was first separated from the Ca matrix prior to analysis using the boron specific resin Amberlite IRA 743 following Foster et al. (2013). The boron isotopic composition was then determined using a sample-standard bracketing routine on a ThermoFisher Scientific Neptune multicollector inductively coupled plasma mass spectrometer (MC-ICPMS) at the University of Southampton (following Foster et al., 2013). The relationship between $\delta^{11}\text{B}$ of CaCO_3 and pH is very closely approximated by the following equation:

$$\text{pH} = \text{p}K_B^* - \log \left(- \frac{\delta^{11}\text{B}_{\text{SW}} - \delta^{11}\text{B}_{\text{CaCO}_3}}{\delta^{11}\text{B}_{\text{SW}} - \alpha_B \cdot \delta^{11}\text{B}_{\text{CaCO}_3} - 1000 \cdot (\alpha_B - 1)} \right) \quad (1)$$

Where $\text{p}K_B^*$ is the equilibrium constant, dependent on salinity, temperature, pressure and seawater major ion composition (i.e., [Ca] and [Mg]), α_B is the fractionation factor between the two boron species and $\delta^{11}\text{B}_{\text{sw}}$ is the boron isotope composition of seawater. Here we use the fractionation factor of 1.0272, calculated from spectrophotometric measurements (Klochko et al., 2006). No temperature correction was applied as a number of recent studies suggest that it is not significant over our investigated temperature range (Rae et al. 2011; Henahan et al., 2013; Martínez-Botí et al. (2015b); Kaczmarek et al. 2016). Although the $\delta^{11}\text{B}$ of foraminifera correlates well with pH and hence $[\text{CO}_2]_{\text{aq}}$, the $\delta^{11}\text{B}_{\text{calcite}}$ is often not exactly equal to $\delta^{11}\text{B}_{\text{borate}}$ (Sanyal et al., 2001; Foster, 2008; Henahan et al., 2013). The planktic species used to construct the benthic-planktic pairs changes through time, as a single species is not available for the entire Neogene (this study; Foster et al., 2012; Martínez-Botí et al., 2015a, and a follow up study by Sosdian et al.). Here *Globigerinoides ruber* is used for 0 to 3 Ma, *Trilobatus sacculifer* (formally *Globigerinoides sacculifer* and including *Trilobatus trilobus*; Hembleden et al., 1987; Spezzaferri et al., 2015) for 0 to 20 Ma and *Globigerina praebulloides* for 22 to 23 Ma. The calibration for *G. ruber* (300-355 μm) is derived from culturing data supported by core top data (Henahan et al., 2013). The *T. sacculifer* calibration (300-355 μm) is from a follow up

r.greenop 1/12/2016 18:14

Deleted: B

r.greenop 1/12/2016 18:14

Deleted: (OH)

r.greenop 1/12/2016 18:14

Deleted: 4

r.greenop 25/11/2016 14:17

Deleted: Martínez-Botí

r.greenop 1/12/2016 17:41

Deleted: Sosdian et al., in prep

203 | [study by](#) Sosdian et al., where the *T. sacculifer* calibration of Sanyal et al., (2001) is
 204 | used with a modified intercept so that it passes through the core top value for *T.*
 205 | *sacculifer* (300–355 µm) from ODP Hole 999A (Seki et al., 2010). Unlike the
 206 | asymbiotic modern *G. bulloides*, *G. praebulloides* appears to be symbiotic at least in
 207 | the latest Oligocene (Pearson and Wade, 2009). Therefore, we apply the *T. sacculifer*
 208 | (300–355µm) calibration to this species. For *T. sacculifer* (500–600µm) between 0
 209 | and 1 Ma, we use the calibration from Martínez-Botí et al. (2015b) where the
 210 | calibration of Sanyal et al. (2001) measured using NTIMS is corrected for the offset
 211 | between MC-ICPMS and NTIMS using a comparison of core-top *T. sacculifer*
 212 | measured by the two different methods from adjacent sites (Foster, 2008; Sanyal et
 213 | al., 1995). In order to constrain deep-water pH, analysis was conducted on benthic
 214 | foraminifera *Cibicidoides wuellerstorfi* or *Cibicidoides mundulus* depending on
 215 | which species were most abundant in each sample. The $\delta^{11}\text{B}$ of both *Cibicidoides*
 216 | species shows no offset from the theoretical $\delta^{11}\text{B}$ of the borate ion and therefore no
 217 | calibration is needed to adjust for species-specific offsets (Rae et al., 2011).

r.greenop 1/12/2016 17:42

Deleted: .. (in prep)

218 | As mentioned above, in addition to $\delta^{11}\text{B}_{\text{calcite}}$, temperature, salinity, water depth
 219 | (pressure) and seawater major ion composition are also needed to calculate pH from
 220 | $\delta^{11}\text{B}$. We use the MyAMI specific ion interaction model (Hain et al., 2015) to
 221 | calculate the appropriate equilibrium constants based on existing [Ca] and [Mg]
 222 | reconstructions (Horita et al., 2002; Brennan et al., 2013). Sea surface temperature
 223 | (SST) is calculated from tandem Mg/Ca analyses on an aliquot of the $\delta^{11}\text{B}$ sample
 224 | (with a conservative 2σ uncertainty of 2°C). Adjustments were made for changes in
 225 | Mg/Ca_{sw} using the records of Horita et al. (2002) and Brennan et al. (2013), and
 226 | correcting for changes in dependence on Mg/Ca_{sw} following Evans and Müller (2012)
 227 | using $H = 0.41$ calculated from *T. sacculifer* (where H describes the power
 228 | relationship between test Mg/Ca incorporation and Mg/Ca_{sw}; Delaney et al., 1985;
 229 | Hasiuk and Lohmann, 2010; Evans and Müller, 2012) using the equations:

r.greenop 25/11/2016 14:18

Deleted: wuellerstorfi

r.greenop 25/11/2016 14:19

Deleted: u

r.greenop 25/11/2016 14:20

Deleted: u

$$\text{Mg/Ca}_{\text{sw.c}} = (\text{Mg/Ca}_{\text{sw.a}} / \text{Mg/Ca}_{\text{sw.m}})^{0.41} \quad (2)$$

230 | Where $\text{Mg/Ca}_{\text{sw.c}}$ is the correction factor applied to the temperature equation for
 231 | changing Mg/Ca_{sw} , $\text{Mg/Ca}_{\text{sw.a}}$ is the estimated Mg/Ca_{sw} for the age of the sample and
 232 | $\text{Mg/Ca}_{\text{sw.m}}$ is modern Mg/Ca_{sw} . Temperature is then calculated using the generic

237 planktic foraminifera calibration of Anand et al. (2003) and including a correction
238 factor for Mg/Ca_{sw} .

$$Temperature = \ln(Mg/Ca_{test}/(0.38 * Mg/Ca_{sw.c}))/0.09 \quad (3)$$

239 Mg/Ca analysis was conducted on a small aliquot of the sample dissolved for isotope
240 analysis at the University of Southampton using a ThermoFisher Scientific Element 2
241 XR. Al/Ca was also measured to assess the competency of the sample cleaning.
242 Because of complications with the Mg/Ca-temperature proxy in *Cibicidoides* species
243 (Elderfield et al., 2006), bottom water temperatures (BWTs) are estimated here by
244 taking the global secular temperature change from the Mg/Ca temperature
245 compilation of Cramer et al. (2011), using the calibration of Lear et al. (2010) and
246 applying this change to the modern bottom water temperature at each site taken from
247 the nearest GLODAP site (with a conservative 2σ uncertainty of 2°C). Salinity is held
248 constant at modern values determined from the nearest GLODAP site (2σ uncertainty
249 of 2 ‰ uncertainty) for the entire record. Note that temperature and salinity have
250 little influence on the calculated pH and the uncertainty in $\delta^{11}\text{B}_{sw}$ is dominated by the
251 uncertainty in the $\delta^{11}\text{B}$ measurement and the estimate of the pH gradient.

252 The majority of the $\delta^{13}\text{C}$ data were measured at Cardiff University on a
253 ThermoFinnigan MAT 252 coupled with a Kiel III carbonate device for automated
254 sample preparation. Additional samples were measured on a gas source mass
255 spectrometer Europa GEO 20-20, University of Southampton equipped with
256 automated carbonate preparation device and on a Finnigan MAT 253 gas isotope
257 ratio mass spectrometer connected to a Kiel IV automated carbonate preparation
258 device at the Zentrum für Marine Tropenökologie (ZMT), Bremen. The Pliocene
259 benthic $\delta^{13}\text{C}$ from Site 999 were taken from the nearest sample in Haug and
260 Tiedemann, (1998). In almost all cases $\delta^{13}\text{C}$ was analysed on the same foraminiferal
261 species as $\delta^{11}\text{B}$ and Mg/Ca (38/44 samples). Where this was not possible another
262 surface dweller/benthic foraminifera was used from the same depth habitat. *C.*

263 | *wuellerstorfi* or *C. mundulus* were measured in all cases for benthic $\delta^{13}\text{C}$. Stable
264 isotope results are reported relative to the Vienna Pee Dee belemnite (VPDB)
265 standard. We use a carbon isotope vital effect for *G. ruber* (+0.94 ‰; Spero et al.,
266 2003), *T. sacculifer*/*G. praebulloides* (+0.46 ‰; Spero et al., 2003; Al-Rousan et al.,
267 | 2004;), *C. mundulus* (+0.47 ‰; McCorkle et al., 1997) and *C. wuellerstorfi* (+0.1 ‰;

r.greenop 25/11/2016 14:18

Deleted: wuellerstorfi

r.greenop 25/11/2016 14:18

Deleted: wuellerstorfi

270 McCorkle et al., 1997) to calculate the $\delta^{13}\text{C}$ of dissolved inorganic carbon (DIC).

271 2.3 Carbon isotopes as a proxy for vertical ocean pH gradient

272 The use of $\delta^{13}\text{C}$ in foraminiferal calcite to estimate the surface to deep pH gradient
273 requires knowledge of the slope of the pH- $\delta^{13}\text{C}$ relationship in the past. In this section
274 we briefly outline the main factors that contribute to the pH- $\delta^{13}\text{C}$ relationship in order
275 to underpin our analysis of extensive carbon cycle model simulations.

276 The production, sinking and sequestration into the ocean interior of low- $\delta^{13}\text{C}$ organic
277 carbon via the soft-tissue component of the biological pump leads to a broad
278 correlation between $\delta^{13}\text{C}$, $[\text{CO}_3^{2-}]$ and macronutrients in the ocean (e.g., Hain et al.,
279 2014a). The remineralization of this organic matter decreases $\delta^{13}\text{C}$ and titrates $[\text{CO}_3^{2-}]$
280 thereby reducing pH, while nutrient concentrations are increased. In waters that have
281 experienced more soft tissue remineralization both pH and $\delta^{13}\text{C}$ will be lower (Fig.
282 5a,b), and this is the dominant reason for the positive slope between $\delta^{13}\text{C}$ and pH in
283 the modern ocean (e.g., Foster et al., 2012; Fig. 5c).

284 Another significant factor affecting the spatial distribution of both $\delta^{13}\text{C}$ and pH is
285 seawater temperature, which affects both the equilibrium solubility of DIC and the
286 equilibrium isotopic composition of DIC. Warmer ocean waters have decreased
287 equilibrium solubility of DIC and so increased local $[\text{CO}_3^{2-}]$ and pH (Goodwin and
288 Lauderdale, 2013), while warmer waters have relatively low equilibrium $\delta^{13}\text{C}$ values
289 (Lynch-Stieglitz et al, 1995). This means that a spatial gradient in temperature acts to
290 drive $\delta^{13}\text{C}$ and pH in opposite directions: warmer waters tend to have higher pH but
291 lower $\delta^{13}\text{C}$. These opposing temperature effects act to reduce the pH difference
292 between two points with greatly different temperature to below the value expected
293 based on $\delta^{13}\text{C}$ alone. In other words, when using $\delta^{13}\text{C}$ differences to estimate the pH
294 gradient between the warm low latitude surface and cold deep waters the appropriate
295 $\Delta\text{pH}-\Delta\delta^{13}\text{C}$ gradient will be less than expected when only considering the effect of
296 organic carbon production, sinking and sequestration. For this reason, in our
297 modeling analysis we focus on the warm-surface to cold-bottom $\Delta\text{pH}/\Delta\delta^{13}\text{C}$ rather
298 than the slope of the overall pH- $\delta^{13}\text{C}$ relationship, with the latter expected to be
299 greater than the former.

r.greenop 4/12/2016 09:56

Moved down [1]: (e.g., Hain et al., 2014a)

r.greenop 4/12/2016 09:56

Moved (insertion) [1]

r.greenop 4/12/2016 09:56

Deleted: so as to reduce

r.greenop 4/12/2016 09:56

Deleted: which

r.greenop 4/12/2016 09:56

Deleted: cause

r.greenop 4/12/2016 09:56

Deleted: That is

r.greenop 4/12/2016 10:00

Deleted: relationship

r.greenop 4/12/2016 09:59

Deleted: effect of the biological pump

307 In the modern ocean, and for the preceding tens of millions of years, the two
 308 dynamics described above are likely dominant in setting spatial variation in $\delta^{13}\text{C}$ and
 309 pH (and $[\text{CO}_3^{2-}]$). However, other processes will have a minor effect on either pH or
 310 $\delta^{13}\text{C}$. For instance, the dissolution of CaCO_3 shells increases $[\text{CO}_3^{2-}]$ and pH
 311 (Broecker and Peng, 1982), but does not significantly affect $\delta^{13}\text{C}$ (Zeebe and Wolf-
 312 Gladrow, 2001). Moreover, the long timescale of air/sea isotopic equilibration of CO_2
 313 combined with kinetic isotope fractionation during net carbon transfer is an important
 314 factor in setting the distribution of $\delta^{13}\text{C}$ on a global ocean scale (Galbraith et al.,
 315 2015; Lynch-Stieglitz et al., 1995), while the effect of CO_2 disequilibrium on $[\text{CO}_3^{2-}]$
 316 and pH is modest (Goodwin and Lauderdale, 2013).

317

318 2.4 Modelling the pH to $\delta^{13}\text{C}$ relationship

319 After correcting for the shift in $\delta^{13}\text{C}$ due to anthropogenic activity, or Suess effect
 320 (Keeling 1979), modern [global](#) ocean observations demonstrate a near-linear
 321 relationship between global ocean data of [in situ seawater](#) pH and $\delta^{13}\text{C}$ DIC with a
 322 slope of 0.201 ± 0.005 (2σ) (Foster et al., 2012; Fig 5c.) This empirically determined
 323 slope might well have been different in past oceans with very different nutrient
 324 cycling, carbon chemistry and circulation compared to today, and it does not
 325 appropriately represent the temperature effect described above (i.e., warm-surface to
 326 cold-bottom water $\Delta\text{pH}/\Delta\delta^{13}\text{C}$). Here we use an ensemble approach with two
 327 independent carbon cycle models to investigate changes in the $\Delta\text{pH}/\Delta\delta^{13}\text{C}$ regression.
 328 Below we provide pertinent information on the GENIE and CYCLOPS model
 329 experiments:

330 We use the Earth System model GENIE-1 (Edwards and Marsh, 2005; Ridgwell et al.
 331 2007) to assess the robustness of the ΔpH -to- $\Delta\delta^{13}\text{C}$ relationship and its sensitivity to
 332 physical and biogeochemical ocean forcing. The configuration used here is closely
 333 related to that of Holden et al. (2013), in which the controls on oceanic $\delta^{13}\text{C}$
 334 distribution were assessed, with an energy and moisture balance in the atmosphere,
 335 simple representations of land vegetation and sea ice, and frictional geostrophic
 336 ocean physics. In each of 16 vertical levels in the ocean, increasing in thickness with
 337 depth, there are 36×36 grid cells (10° in longitude and nominally 5° in latitude, with

r.greenop 4/12/2016 10:00

Deleted:

r.greenop 4/12/2016 10:32

Deleted: seawater

340 higher resolution at low latitudes). Modern ocean bathymetry and land topography is
341 applied in all simulations. The ocean biogeochemical scheme (Ridgwell et al. 2007)
342 is based on conversion of DIC to organic carbon associated with phosphate uptake
343 with fixed P:C:O stoichiometry. Organic carbon and nutrients are remineralized
344 according to a remineralization profile with a pre-defined *e*-folding depth scale. This
345 depth scale, as well as the rain ratio of inorganic to organic carbon in sinking
346 particulate matter, is among the parameters examined in the sensitivity study. In these
347 simulations, there is no interaction with sediments. As a result of this, the steady state
348 solutions reported here are reached within the 5000-year simulations, but [they](#) are not
349 consistent with being in secular steady state with regard to the balance of continental
350 weathering and ocean CaCO₃ burial.

351 The sensitivity study consists of seven sets of experiments, each varying a single
352 model parameter relative to the control simulation with preindustrial atmospheric
353 *p*CO₂. This enables us to assess which processes, if any, are capable of altering the
354 oceanic relationship between $\Delta p\text{H}$ and $\Delta \delta^{13}\text{C}$ relationship, and the uncertainty in the
355 predictive skill of this relationship due to spatial variability. These experiments are
356 therefore exploratory in nature and intended to study plausible range rather than
357 determine magnitude of past changes. The seven parameters varied are (1) the ocean
358 alkalinity reservoir; (2) the ocean's carbon reservoir; (3) the parameter "S. Lim gas
359 exchange" which blocks air-sea gas exchange south of the stated latitude, significant
360 here because of the dependence of $\delta^{13}\text{C}$ on surface disequilibrium (Galbraith et al.,
361 2015); (4) inorganic to organic carbon rain ratio, controlling the relationship between
362 DIC and alkalinity distributions; (5) "Antarctic shelf FWF", a freshwater flux
363 adjustment (always switched off in control experiments with GENIE) facilitating the
364 formation of brine rich waters, which produces a high-salinity poorly-ventilated deep
365 ocean at high values; (6) "Atlantic-Pacific FWF", a freshwater flux adjustment
366 equivalent to freshwater hosing, leading to a shut-down of the Atlantic meridional
367 overturning circulation at low values; (7) remineralization depth-scale of sinking
368 organic matter, which affects the vertical gradient both of pH and $\delta^{13}\text{C}$. A wide range
369 of parameter values is chosen for each parameter in order to exceed any plausible
370 changes within the Cenozoic.

r.greenop 4/12/2016 10:01

Deleted: 's

r.greenop 4/12/2016 10:01

Deleted: -to-

For the second exploration of the controls on the slope of [the](#) $\Delta\text{pH}-\Delta\delta^{13}\text{C}$ relationship we use the CYCLOPS biogeochemical 18-box model that includes a dynamical lysocline, a subantarctic zone surface box and a polar Antarctic zone box (Sigman et al., 1998; Hain et al., 2010, 2014b). The very large model ensemble with 13,500 individual model scenarios is designed to capture the full plausible range of (a) glacial/interglacial carbon cycle states by sampling the full solution space of Hain et al. (2010), and (b) reconstructed secular changes in seawater [Ca] (calcium concentration), carbonate compensation depth (CCD), weathering and atmospheric CO_2 (Table 1). The following seven model parameters are systematically sampled to set the 13,500 model scenarios: (1) shallow versus deep Atlantic meridional overturning circulation represented by modern reference north Atlantic deep water (NADW) versus peak glacial North Atlantic intermediate water (GNAIW) circulation; (2) iron-driven changes in nutrient drawdown in the subantarctic zone of the Southern Ocean; (3) changes in nutrient drawdown of the polar Antarctic; (4) changes in vertical exchange between the deep Southern Ocean and the polar Antarctic surface; (5) range in seawater [Ca] concentration from 1x to 1.5x modern as per reconstructions (Horita et al., 2002); (6) Pacific CCD is set to the range of 4.4-4.9 km via changes in the weathering flux, as per sedimentological evidence (Pälike et al., 2012); (7) atmospheric CO_2 is set from 200 ppm to 1000 ppm by changes in the ‘weatherability’ parameter of the silicate weathering mechanism. The ensemble spans predicted bulk ocean DIC between 1500 and 4500 $\mu\text{mol/kg}$, a wide range of ocean pH and CaCO_3 saturation states consistent with the open system weathering cycle, and widely different states of the oceanic biological pump. All 13,500 model scenarios are run for two million years after every single ‘weatherability’ adjustment, part of the CCD inversion algorithm, guaranteeing the specified CCD depth and steady state with regard to the balance of continental weathering and ocean CaCO_3 burial for the final solution (unlike the GENIE simulations CaCO_3 burial was entirely neglected due to computational cost of the long model integrations it would require). The inverse algorithm typically takes at least ten steps to convergence, resulting in ~300 billion simulated years for this ensemble. [This range of modelling parameters was chosen to exceed the range of carbonate system and ocean circulation changes that can be expected for the Neogene based on records of \[Ca\] and \[Mg\] \(Horita et](#)

r.greenop 4/12/2016 10:02

Deleted:

r.greenop 4/12/2016 10:02

Deleted: 's

al., 2002), CCD changes (Pälike et al., 2012), atmospheric CO₂ (Beerling and Royer, 2011) and records of glacial-interglacial circulation change (Curry and Oppo, 2005).

2.5 Assessing uncertainty

$\delta^{11}\text{B}_{\text{sw}}$ uncertainty was calculated using a Monte Carlo approach where pH was calculated for deep and surface waters at each time slice using a random sampling (n=10000) of the various input parameters within their respective uncertainties as represented by normal distributions. These uncertainties (2σ uncertainty in parentheses) are: temperature ($\pm 2^\circ\text{C}$), salinity (± 2 units on the practical salinity scale) [Ca] (± 4.5 mmol/kg), [Mg], (± 4.5 mmol/kg), $\delta^{11}\text{B}_{\text{planktic}}$ (± 0.15 - 0.42‰) and $\delta^{11}\text{B}_{\text{benthic}}$ (± 0.21 - 0.61‰). For the estimate of the surface to sea floor pH gradient we use the central value of the ΔpH -to- $\Delta\delta^{13}\text{C}$ relationship diagnosed from our CYCLOPS and GENIE sensitivity experiments (i.e., 0.175‰ , see section 3.2 below) and then we assign a ± 0.05 uncertainty range with a uniform probability (rather than a normal distribution) to the resulting surface to sea floor ΔpH estimate (see also Table 2). Thus, the magnitude of this nominal uncertainty is equivalent to a 0.14‰ to 0.21‰ $\Delta\text{pH}/\Delta\delta^{13}\text{C}$ uncertainty range that spans the vast majority of our CYCLOPS and GENIE simulations, and the prediction error (RMSE) of fitting a linear relationship to the GENIE pH and $\delta^{13}\text{C}$ output (see section 3.2 below). The uncertainty in the $\delta^{11}\text{B}$ measurements is calculated from the long-term reproducibility of Japanese Geological Survey *Porites* coral standard (JCP; $\delta^{11}\text{B}=24.3\text{‰}$) at the University of Southampton using the equations:

$$2\sigma = 2.25 \exp^{-23.01[^{11}\text{B}]} + 0.28 \exp^{-0.64[^{11}\text{B}]} \quad (4)$$

$$2\sigma = 33450 \exp^{-168.2[^{11}\text{B}]} + 0.311 \exp^{-1.477[^{11}\text{B}]} \quad (5)$$

where $[^{11}\text{B}]$ is the intensity of ^{11}B signal in volts and equation (4) and equation (5) used with $10^{11} \Omega$ and $10^{12} \Omega$ resistors, respectively.

From the 10,000 Monte Carlo ensemble solutions of our 22 benthic-planktic pairs we construct 10,000 randomized records of $\delta^{11}\text{B}_{\text{sw}}$ as a function of time. Each of these randomized $\delta^{11}\text{B}_{\text{sw}}$ records are subjected to smoothing using the locally weighted scatterplot smoothing (LOWESS) algorithm with a smoothing parameter (span) of 0.7. The purpose of the smoothing is to put some controls on the rate at which the

r.greenop 1/12/2016 18:15

Deleted:

438 resulting individual Monte Carlo $\delta^{11}\text{B}_{\text{sw}}$ records are allowed to change, which in
 439 reality is limited by the seawater boron mass balance ($\sim 0.1\text{‰}$ per million years;
 440 boron residence time is 11-17 million years; Lemarchand et al., 2000). Our choice of
 441 smoothing parameter allows for some of the individual Monte Carlo records to
 442 change as fast as $\sim 1\text{‰}$ per million years, although in reality the average rate of
 443 change is much smaller than this (see section 3.3). Consequently this method
 444 removes a significant amount of uncorrelated stochastic noise (resulting from the
 445 uncertainty in our input parameters) while not smoothing away the underlying signal.
 446 As a result of anomalously low $\delta^{11}\text{B}$ differences ($< 1\text{‰}$) between benthic and planktic
 447 pairs, two pairs at 8.68 Ma and 19 Ma were discarded from the smoothing. It may be
 448 possible that preservation is not so good within these intervals and the planktic
 449 foraminifera are affected by partial dissolution (Seki et al., 2010). The spread of the
 450 ensemble of smoothed $\delta^{11}\text{B}_{\text{sw}}$ curves represents the combination of the compounded,
 451 propagated uncertainties of the various inputs (i.e., Monte Carlo sampling) with the
 452 additional constraint of gradual $\delta^{11}\text{B}_{\text{sw}}$ change over geological time imposed by the
 453 inputs and outputs of boron to the ocean and the total boron inventory (i.e., the
 454 smoothing of individual Monte Carlo members. Various statistical properties (i.e.,
 455 mean, median, standard deviation (σ), various quantiles) of this $\delta^{11}\text{B}_{\text{sw}}$ reconstruction
 456 were evaluated from the ensemble of smoothed $\delta^{11}\text{B}_{\text{sw}}$ records. Generally, for any
 457 given benthic-planktic pair the resulting $\delta^{11}\text{B}_{\text{sw}}$ estimates are not perfectly normally
 458 distributed and thus we use the median as the metric for the central tendency (i.e.,
 459 placement of marker in Figure 10).

460 3. Results and Discussion

461 3.1 $\delta^{11}\text{B}$ benthic and planktic data

462 Surface and deep-ocean, $\delta^{11}\text{B}$ broadly show a similar, but inverse, pattern to $\delta^{13}\text{C}$ and
 463 temperature throughout the Neogene (Fig. 6). The $\delta^{11}\text{B}$ benthic record decreases from
 464 $\sim 15\text{‰}$ at 24 Ma to a minimum of 13.28‰ at 14 Ma before increasing to $\sim 17\text{‰}$ at
 465 present day (Fig. 6). This pattern and the range of values in benthic foraminiferal $\delta^{11}\text{B}$
 466 is in keeping with previously published Neogene $\delta^{11}\text{B}$ benthic records measured
 467 using NTIMS (Raitzsch and Hönisch, 2013), suggesting that our deep-water $\delta^{11}\text{B}$
 468 record is representative of large scale pH changes in the global ocean. While the

r.greenop 4/12/2016 10:03

Deleted: in the core

r.greenop 4/12/2016 10:04

Deleted: B,

r.greenop 4/12/2016 10:04

Deleted: $\delta^{13}\text{C}$ and temperature

r.greenop 4/12/2016 10:04

Deleted: one another

r.greenop 1/12/2016 18:15

Deleted:

474 surface $\delta^{11}\text{B}_{\text{planktic}}$ remained relatively constant between 24 and 11 Ma at $\sim 16\text{‰}$, there
 475 is a significant increase in $\delta^{11}\text{B}$ between the middle Miocene and present (values
 476 increase to $\sim 20\text{‰}$) (Fig. 6b). The reconstructed surface water temperatures show a
 477 long-term decrease through the Neogene from $\sim 28^\circ\text{C}$ to 24°C , aside from during the
 478 Miocene Climatic Optimum (MCO) where maximum Neogene temperatures are
 479 reached (Fig. 6c). Following Cramer et al. (2011) deep-water temperatures decrease
 480 from $\sim 12^\circ\text{C}$ to 4°C at the present day and similarly show maximum temperatures in
 481 the MCO. Surface and deep-water $\delta^{13}\text{C}_{\text{DIC}}$ both broadly decrease through the Neogene
 482 and appear to covary on shorter timescales (Fig. 6e, f).

483

484 3.2 The relationship between $\delta^{13}\text{C}$ and pH gradients

485 | [In](#) the global modern ocean data, after accounting for the anthropogenic carbon, the
 486 empirical relationship between *in situ* pH and DIC $\delta^{13}\text{C}$ is well described by a linear
 487 function with a slope of 0.201 ± 0.005 (2σ) (Fig. 5; Foster et al., 2012). However, this
 488 slope is only defined by surface waters in the North Atlantic due to a current lack of
 489 modern data where the impact of the Suess effect has been corrected (Olsen and
 490 Ninneman, 2010). Consequently we are not currently able to determine the slope
 491 between the warm-surface and cold-deep ocean in the modern ocean at our sites.
 492 Instead, here we use the two modeling experiments to define this slope. In the control
 493 | GENIE experiment (green star; Fig. 7), the central value for the slope of the pH/ $\delta^{13}\text{C}$
 494 relationship is slightly greater than 0.2‰ for the full 3D data regression (not shown)
 495 and about 0.175‰ for the warm-surface-to-cold-deep ΔpH -to- $\Delta\delta^{13}\text{C}$ relationship
 496 (Fig. 7) – consistent with theory for the effect of temperature gradients (see section
 497 2.3). For both ways of analysing the GENIE output the prediction uncertainty of the
 498 regressions, the root-mean-squared error (RMSE), is $\sim 0.05\text{‰}$ under most conditions
 499 | (open red circles in Fig. 7), with the exception of [cases](#) where large changes in either
 500 DIC or ALK [yield](#) somewhat larger changes in the relationship between pH and $\delta^{13}\text{C}$
 501 (see below). In our CYCLOPS model ensemble, the central value of the slopes of the
 502 full 3D pH/ $\delta^{13}\text{C}$ regressions and of the warm-surface-to-cold-deep $\Delta\text{pH}/\Delta\delta^{13}\text{C}$ is
 503 0.2047‰ (1σ of 0.0196‰ ; Fig. 8a) and 0.1797‰ (1σ of 0.0213‰ ; Fig. 8b),
 504 respectively. If we restrict our analysis of the CYCLOPS ensemble to only the

r.greenop 4/12/2016 10:05

Deleted: As noted above, in

r.greenop 4/12/2016 10:05

Deleted:

r.greenop 4/12/2016 10:05

Deleted: result in

508 Atlantic-basin warm-surface-to-cold-deep $\Delta p\text{H}/\Delta\delta^{13}\text{C}$, where most of our samples
 509 come from, we find a relationship of only 0.1655/‰ (1 σ of 0.0192/‰; Fig.8c). That
 510 is, overall, we find near-perfect agreement between modern empirical data and our
 511 GENIE and CYCLOPS experiments. Encouraged by this agreement we select the
 512 warm-surface-to-cold-deep $\Delta p\text{H}/\Delta\delta^{13}\text{C}$ central value of 0.175/‰ to estimate the
 513 surface/sea floor pH difference from the planktic/benthic foraminifera $\delta^{13}\text{C}$
 514 difference. To account for our ignorance as to the accurate value of $\Delta p\text{H}/\Delta\delta^{13}\text{C}$ in the
 515 modern ocean, its [temporal](#) changes over the course of the study interval and the
 516 inherent prediction error from using a linear $\Delta p\text{H}$ -to- $\Delta\delta^{13}\text{C}$ relationship, we assign a
 517 nominal uniform uncertainty range of ± 0.05 around the central $\Delta p\text{H}$ estimate for the
 518 purpose of Monte Carlo uncertainty propagation. Our analysis also suggests that
 519 where surface-to-thermocline planktic/planktic gradients are employed, the plausible
 520 $\Delta p\text{H}/\Delta\delta^{13}\text{C}$ range should be significantly higher than applied here to account for the
 521 relatively lower temperature difference. Based on the appropriate $\Delta p\text{H}/\Delta\delta^{13}\text{C}$
 522 relationship we reconstruct a time varying surface-to-deep pH gradient, which
 523 ranges between 0.14 and 0.35 pH units over our study interval (Fig. 9) and apply a
 524 flat uncertainty of ± 0.05 . The reconstructed pH gradient remains broadly within the
 525 range of the modern values (0.19 to 0.3) although there is some evidence of multi-
 526 million year scale variability ([Fig. 9](#)).

527 As a caveat to our usage of the $\Delta p\text{H}$ -to- $\Delta\delta^{13}\text{C}$ relationship we point to changes of that
 528 relationship that arise in our GENIE sensitivity experiments where carbon and
 529 alkalinity inventories are manipulated, which can yield values outside of what is
 530 plausible. We note that our CYCLOPS ensemble samples a very much wider range of
 531 carbon and alkalinity inventories with $\Delta p\text{H}/\Delta\delta^{13}\text{C}$ remaining inside that range. While
 532 CYCLOPS simulates the balance between weathering and CaCO_3 burial, which is
 533 known to neutralize sudden carbon or alkalinity perturbations on timescales much
 534 less than one million years, the configuration used for our GENIE simulations does
 535 not and is therefore subject to states of ocean carbon chemistry that can safely be
 536 ruled out for our study interval and likely for most of the Phanerozoic. The differing
 537 outputs from CYCLOPS and GENIE in the DIC and ALK experiments [shows](#) that
 538 $\Delta p\text{H}/\Delta\delta^{13}\text{C}$ depends on background seawater acid/base chemistry, in ways that are
 539 not yet fully understood. That said, the generally coherent nature of our results
 540 confirms [that](#) we likely constrain the plausible range of $\Delta p\text{H}/\Delta\delta^{13}\text{C}$ for at least the

r.greenop 25/11/2016 14:29
Deleted: ,

r.greenop 4/12/2016 10:07
Deleted: ,

r.greenop 4/12/2016 10:07
Deleted: in order

r.greenop 4/12/2016 10:07
Deleted:

r.greenop 4/12/2016 10:07
Deleted:

r.greenop 1/12/2016 18:16
Deleted:

r.greenop 4/12/2016 10:07
Deleted: does highlight

r.greenop 4/12/2016 10:08
Deleted: actually

549 Neogene, if not the entire Cenozoic, outside of extreme events such as the
550 Palaeocene-Eocene Thermal Maximum.

551

552 3.3 $\delta^{11}\text{B}_{\text{sw}}$ record through the Neogene

553 Using input parameter uncertainties as described in section 2.5 yields individual
554 Monte Carlo member $\delta^{11}\text{B}_{\text{sw}}$ estimates between 30 ‰ and 43.5 ‰ at the overall
555 extreme points and typically ranging by ~10 ‰ (dashed in Fig. 10a) for each time
556 point, suggesting that the uncertainties we assign to the various input parameters are
557 generous enough not to predetermine the quantitative outcomes. However, for each
558 planktic/benthic time point most individual Monte Carlo $\delta^{11}\text{B}_{\text{sw}}$ estimates fall into a
559 much narrower central range (~1 ‰ to 4 ‰; thick black line showing interquartile
560 range in Fig. 10a). The $\delta^{11}\text{B}_{\text{sw}}$ for Plio-Pleistocene time-points cluster around ~40 ‰
561 while middle/late Miocene values cluster around ~36.5 ‰. The estimates at
562 individual time points are completely independent from each other, such that the
563 observed clustering is strong evidence for an underlying long-term signal in our data,
564 albeit one that is obscured by the uncertainties involved in our individual $\delta^{11}\text{B}_{\text{sw}}$
565 estimates. The same long-term signal is also evident when pooling the individual
566 Monte Carlo member $\delta^{11}\text{B}_{\text{sw}}$ estimates into 8 million year bins and evaluating the
567 mean and spread (2σ) in each bin (Fig. 10b). This simple treatment highlights that
568 there is a significant difference between our Plio-Pleistocene and middle Miocene
569 data bins at the 95% confidence level and that $\delta^{11}\text{B}_{\text{sw}}$ appears to also have been
570 significantly lower than modern during the early Miocene.

571 3.3.1 Data smoothing

572 The ~1 to 4 ‰ likely ranges for $\delta^{11}\text{B}_{\text{sw}}$ would seem to be rather disappointing given
573 the goal to constrain $\delta^{11}\text{B}_{\text{sw}}$ for pH reconstructions. However, most of that uncertainty
574 is stochastic, random error that is uncorrelated from time point to time point.
575 Furthermore, we know from mass balance considerations that $\delta^{11}\text{B}_{\text{sw}}$ of seawater
576 should not change by more than ~0.1 ‰ per million years (Lemarchand et al., 2000),
577 [because of the size of the oceanic boron reservoir compared the inputs and outputs](#)
578 [\(see Fig. 1\)](#), and we use this as an additional constraint via the LOWESS smoothing
579 we apply to each Monte Carlo time series. One consideration is that every individual

r.greenop 4/12/2016 10:09

Deleted: each and

Monte Carlo $\delta^{11}\text{B}_{\text{sw}}$ estimate is equally likely and the smoothing should therefore target randomly selected individual Monte Carlo $\delta^{11}\text{B}_{\text{sw}}$ estimates, as we do here, rather than smoothing over the likely ranges identified for each time point. In this way the smoothing becomes integral part of our Monte Carlo uncertainty propagation and the spread among the 10,000 individual smoothed $\delta^{11}\text{B}_{\text{sw}}$ curves carries the full representation of propagated input uncertainty conditional on the boron cycle mass balance constraint. A second consideration is that the smoothing should only remove noise, not underlying signal. As detailed above, for this reason the smoothing parameter we choose has enough freedom to allow the $\delta^{11}\text{B}_{\text{sw}}$ change to be dictated by the data, with only the most extreme shifts in $\delta^{11}\text{B}_{\text{sw}}$ removed. We also tested the robustness of the smoothing procedure itself (not shown) and found only marginal changes when changing algorithm (LOESS versus LOWESS, with and without robust option) or when reducing the amount of smoothing (i.e., increasing the allowed rate $\delta^{11}\text{B}_{\text{sw}}$ change). The robustness of our smoothing is further underscored by the good correspondence with the results of simple data binning (Fig.10b).

3.4 Comparison to other $\delta^{11}\text{B}_{\text{sw}}$ records

The comparison of our new $\delta^{11}\text{B}_{\text{sw}}$ record to those previously published reveals that despite the differences in methodology the general trends in the records show excellent agreement. The most dominant common feature of all the existing estimates of Neogene $\delta^{11}\text{B}_{\text{sw}}$ evolution is an increase through time from the middle Miocene to the Plio-Pleistocene (Fig. 11). While the model-based $\delta^{11}\text{B}_{\text{sw}}$ record of Lemarchand et al. (2000) is defined by a monotonous and very steady rise over the entire study interval, all three measurement-based records, including our own, are characterized by a single dominant phase of increase between roughly 12 and 5 Ma. Strikingly, the Pearson and Palmer (2000) record falls almost entirely within our 95% likelihood envelope, overall displaying very similar patterns of long-term change but with a relatively muted amplitude and overall rate of change relative to our reconstruction. Conversely, some of the second-order variations in the reconstruction by Raitzsch and Hönisch (2013) are not well matched by our reconstruction, but the dominant episode of rapid $\delta^{11}\text{B}_{\text{sw}}$ rise following the middle Miocene is in almost perfect

612 agreement. We are encouraged by these agreements resulting from approaches based
613 on very different underlying assumptions and techniques, which we take as indication
614 for an emerging consensus view of $\delta^{11}\text{B}_{\text{sw}}$ evolution over the last 25 Ma and as a
615 pathway towards reconstructing $\delta^{11}\text{B}_{\text{sw}}$ further back in time. Below we discuss in
616 more detail the remaining discrepancies between our new and previously existing
617 $\delta^{11}\text{B}_{\text{sw}}$ reconstructions.

618 The record by Pearson and Palmer (2000) is well correlated to our reconstruction, but
619 especially during the early Miocene there is a notable $\sim 0.5\text{‰}$ offset (Fig. 11). This
620 discrepancy could be due to a number of factors. Firstly, the applicability of this
621 $\delta^{11}\text{B}_{\text{sw}}$ record (derived from $\delta^{11}\text{B}$ data measured using NTIMS) to $\delta^{11}\text{B}$ records
622 generated using the MC-ICPMS is uncertain (Foster et al., 2013). In addition, this
623 $\delta^{11}\text{B}_{\text{sw}}$ record is determined using a fractionation factor of 1.0194 (Kakihana et al.,
624 1977), whereas recent experimental data have shown the value to be higher ($1.0272 \pm$
625 0.0006 , Klochko et al., 2006), although foraminiferal vital effects are likely to mute
626 this discrepancy. Thirdly, given our understanding of the $\delta^{11}\text{B}$ difference between
627 species/size fractions (Foster, 2008; Henahan et al., 2013), the mixed species and size
628 fractions used to make the $\delta^{11}\text{B}$ measurements in that study may have introduced
629 some additional uncertainty in the reconstructed $\delta^{11}\text{B}_{\text{sw}}$. Conversely, there is
630 substantial spread between our three time points during the earliest Miocene, which
631 combined with the edge effect of the smoothing gives rise to a widening uncertainty
632 envelope during the time of greatest disagreement with Pearson and Palmer (2000).
633 This could be taken as indication that our reconstruction, rather than that of Pearson
634 and Palmer, is biased during the early Miocene.

635

636 The $\delta^{11}\text{B}_{\text{sw}}$ record calculated using benthic $\delta^{11}\text{B}$ and assumed deep ocean pH changes
637 (Raitzsch and Hönisch, 2013) is also rather similar to our $\delta^{11}\text{B}_{\text{sw}}$ reconstruction. The
638 discrepancy between the two records in the early Miocene could plausibly be
639 explained by bias in our record (see above) or may in part be as a result of the
640 treatment of surface water pH in the study of Raitzsch and Hönisch (2013) and their
641 assumption of constant surface-deep pH gradient (see Fig 9). The combined output
642 from two carbon cycle box models is used to make the assumption that surface ocean
643 pH near-linearly increased by 0.39 over the last 50 Myrs. The first source of surface

r.greenop 4/12/2016 10:10

Deleted: ,

645 water pH estimates is from the study of Ridgwell et al. (2005), where CO₂ proxy data
 646 including some derived using the boron isotope-pH proxy is used, leading to some
 647 circularity in the methodology. The second source of surface water pH estimates is
 648 from Tyrrell & Zeebe (2004) and based on GEOCARB where the circularity problem
 649 does not apply. While this linear pH increase broadly matches the CO₂ decline from
 650 proxy records between the middle Miocene and present, it is at odds with the CO₂
 651 proxy data during the early Miocene that show CO₂ was lower than the middle
 652 Miocene during this interval (Beerling and Royer, 2011). Consequently the proxy
 653 CO₂ and surface water pH estimates may not be well described by the linear change
 654 in pH applied by Raitzsch and Hönisch (2013) across this interval, potentially
 655 contributing to the discrepancy between our respective $\delta^{11}\text{B}_{\text{sw}}$ reconstructions.

656 Our new $\delta^{11}\text{B}_{\text{sw}}$ record falls within the broad uncertainty envelope of boron mass
 657 balance calculations of Lemarchand et al. (2000), but those modelled values do not
 658 show the same level of multi-million year variability of either Raitzsch and Hönisch
 659 (2013) or our new record, therefore suggesting that the model does not fully account
 660 for aspects of the changes in the ocean inputs and outputs of boron through time on
 661 timescales less than ~10 million years.

662 In line with the conclusions of previous studies (e.g., Raitzsch and Hönisch, 2013),
 663 our data show that the $\delta^{11}\text{B}_{\text{sw}}$ signal in the fluid inclusions (Paris et al., 2010) is most
 664 likely a combination of the $\delta^{11}\text{B}_{\text{sw}}$ and some other factor such as a poorly constrained
 665 fractionation factor between the seawater and the halite. Brine-halite fractionation
 666 offsets of -20‰ to -30‰ and -5‰ are reported from laboratory and natural
 667 environments (Vengosh et al., 1992; Liu et al., 2000). These fractionations and
 668 riverine input during basin isolation will drive the evaporite-hosted boron to low- $\delta^{11}\text{B}$
 669 isotope values such that the fluid inclusion record likely provides a lower limit for the
 670 $\delta^{11}\text{B}_{\text{sw}}$ through time (i.e. $\delta^{11}\text{B}_{\text{sw}}$ is heavier than the halite fluid inclusions of Paris et al.
 671 (2010)). For this halite record to be interpreted directly as $\delta^{11}\text{B}_{\text{sw}}$, a better
 672 understanding of the factor(s) controlling the fractionation during halite formation
 673 and any appropriate correction need to be better constrained.

r.greenop 1/12/2016 18:18

Deleted: .

r.greenop 25/11/2016 14:37

Deleted: are

r.greenop 1/12/2016 18:18

Deleted: .

r.greenop 1/12/2016 18:18

Deleted: ly

r.greenop 4/12/2016 10:10

Deleted: In order f

3.5 Common controls on the seawater isotopic ratios of B, Mg, Ca and Li

Our new record of $\delta^{11}\text{B}_{\text{sw}}$ has some substantial similarities to secular change seen in other marine stable isotope records (Fig. 12). The lithium isotopic composition of seawater ($\delta^7\text{Li}_{\text{sw}}$; Misra and Froelich, 2012) and the calcium isotopic composition of seawater [as recorded in marine barites](#) ($\delta^{44/40}\text{Ca}_{\text{sw}}$; Griffith et al., 2008) both increase through the Neogene, whereas the magnesium isotopic composition of seawater ($\delta^{26}\text{Mg}_{\text{sw}}$) decreases (Pogge von Strandmann et al., 2014) suggesting a similar control on the isotopic composition of all four elements across this time interval (Fig. 12). To further evaluate the correlation between these other marine isotope records and $\delta^{11}\text{B}_{\text{sw}}$, we interpolate and cross-plot $\delta^{11}\text{B}_{\text{sw}}$ and the $\delta^7\text{Li}_{\text{sw}}$, $\delta^{44/40}\text{Ca}_{\text{sw}}$ and $\delta^{26}\text{Mg}_{\text{sw}}$ records. This analysis suggests that the isotopic composition of $\delta^{11}\text{B}_{\text{sw}}$, $\delta^7\text{Li}_{\text{sw}}$, $\delta^{26}\text{Mg}_{\text{sw}}$ and $\delta^{44/40}\text{Ca}_{\text{sw}}$ are well correlated through the Neogene, although there is some scatter in these relationships (Fig. 13). Although the Sr isotope record shows a similar increase during the Neogene (Hodell et al., 1991), we focus our discussion on $\delta^{11}\text{B}_{\text{sw}}$, $\delta^7\text{Li}_{\text{sw}}$, $\delta^{26}\text{Mg}_{\text{sw}}$ and $\delta^{44/40}\text{Ca}_{\text{sw}}$ given that the factors fractionating these stable isotopic systems are similar (see below).

To better constrain the controls on $\delta^{11}\text{B}_{\text{sw}}$, $\delta^7\text{Li}_{\text{sw}}$, $\delta^{26}\text{Mg}_{\text{sw}}$ and $\delta^{44/40}\text{Ca}_{\text{sw}}$ it is instructive to compare the size and isotopic composition of the fluxes of boron, lithium, calcium and magnesium to the ocean (Table 3). The major flux of boron into the ocean is via riverine input (Lemarchand et al., 2000), although some studies suggest that atmospheric input may also play an important role (Park and Schlesinger, 2002). The loss terms are dominated by adsorption onto clays and the alteration of oceanic crust (Spivack and Edmond, 1987; Smith et al., 1995). Similarly, the primary inputs of lithium into the ocean come from hydrothermal sources and riverine input and the main outputs are ocean crust alteration and adsorption onto sediments (Misra and Froelich, 2012). The [three](#) dominant controls on magnesium concentration and isotope ratio in the oceans is the riverine input, ocean crust alteration and dolomitization (Table 3) (Tipper et al., 2006b). The main controls on the amount of calcium in the modern ocean and its isotopic composition is the balance between riverine and hydrothermal inputs and removal through CaCO_3 deposition and alteration of oceanic crust (Fantle and Tipper, 2014, Griffith et al., 2008). Dolomitization has also been cited as playing a potential role in controlling

r.greenop 25/11/2016 12:45

Deleted: two

713 $\delta^{44/40}\text{Ca}_{\text{sw}}$, although the contribution of this process through time is poorly constrained
714 (Griffith et al., 2008).

715 Analysis of the oceanic fluxes of all four ions suggests that riverine input may be an
716 important factor influencing the changing isotopic composition of B, Li, Ca and Mg
717 over the late Neogene (Table 3). In the case of all four elements, a combination of the
718 isotopic ratio of the source rock and isotopic fractionation during weathering
719 processes are typically invoked to explain the isotopic composition of a particular
720 river system. However, in most cases the isotopic composition of the source rock is
721 found to be of secondary importance (Rose et al., 2000; Kısakürek et al., 2005;
722 Tipper et al., 2006b; Millot et al., 2010). For instance, the $\delta^{11}\text{B}$ composition of rivers
723 is primarily dependent on isotopic fractionation during the reaction of water with
724 silicate rocks and to a lesser extent the isotopic composition of the source rock (i.e.
725 the proportion of evaporites and silicate rocks; Rose et al., 2000). While some studies
726 have suggested that the isotopic composition of rainfall within the catchment area
727 may be an important factor controlling the $\delta^{11}\text{B}$ in rivers (Rose-Koga et al., 2006),
728 other studies have shown atmospheric boron to be a secondary control on riverine
729 boron isotope composition (Lemarchand and Gaillardet, 2006). The source rock also
730 appears to have limited influence on the $\delta^7\text{Li}$ composition of rivers and riverine $\delta^7\text{Li}$
731 varies primarily with weathering intensity (Kısakürek et al., 2005; Millot et al.,
732 2010). The riverine input of calcium to the oceans is controlled by the composition of
733 the primary continental crust (dominated by carbonate weathering) and a recycled
734 component, although the relative influence of these two processes is not well
735 understood (Tipper et al., 2006a). In addition, vegetation may also play a significant
736 role in the $\delta^{44/40}\text{Ca}$ of rivers (Fantle and Tipper, 2014). For Mg, the isotopic
737 composition of the source rock is important for small rivers, however, lithology is of
738 limited significance at a global scale in comparison to fractionation in the weathering
739 environment (Tipper et al., 2006b). Given the lack of evidence of source rock as a
740 dominant control on the isotopic composition of rivers, here we focus on some of the
741 possible causes for changes in the isotopic composition and/or flux of riverine input
742 over the Neogene.

743 In this regard, of the four elements discussed here, the Li isotopic system is the most
744 extensively studied. Indeed, the change in $\delta^7\text{Li}_{\text{sw}}$ has already been attributed to an

r.greenop 4/12/2016 10:11

Deleted:

746 increase in the $\delta^7\text{Li}_{\text{sw}}$ composition of the riverine input (Hathorne and James, 2006;
 747 Misra and Froelich, 2012). The causes of the shift in $\delta^7\text{Li}$ riverine have been variably
 748 attributed to: (1) an increase in incongruent weathering of silicate rocks and
 749 secondary clay formation as a consequence of Himalayan uplift (Misra and Froelich,
 750 2012; [Li and West, 2014](#)), (2) a reduction in weathering intensity (Hathorne and
 751 James, 2006; Froelich and Misra, 2014; [Wanner et al., 2014](#)), (3) an increase in
 752 silicate weathering rate (Liu et al., 2015), 4) an increase in the formation of
 753 floodplains and the increased formation of secondary minerals (Pogge von
 754 Strandmann and Henderson, 2014) and (5) a climatic control on soil production rates
 755 (Vigier and Godderis, 2015). In all five cases the lighter isotope of Li is retained on
 756 land in clay and secondary minerals. A mechanism associated with either an increase
 757 in secondary mineral formation or the retention of these minerals on land is also
 758 consistent across Mg, Ca and B isotope systems. For instance, clay minerals are
 759 preferentially enriched in the light isotope of B (Spivack and Edmond, 1987; Deyhle
 760 and Kopf, 2004; Lemarchand and Gaillardet, 2006) and Li (Pistiner and Henderson,
 761 2003) and soil carbonates and clays are preferentially enriched in the light isotope of
 762 Ca (Tipper et al., 2006a; Hindshaw et al., 2013; Ockert et al., 2013). The formation of
 763 secondary silicate minerals, such as clays, is assumed to preferentially take up the
 764 heavy Mg isotope into the solid phase (Tipper et al., 2006a; Tipper et al., 2006b;
 765 Pogge von Strandmann et al., 2008; Wimpenny et al., 2014), adequately explaining
 766 the inverse relationship between $\delta^{11}\text{B}_{\text{sw}}$ and $\delta^{26}\text{Mg}_{\text{sw}}$. Consequently the increased
 767 formation or retention on land of secondary minerals would alter the isotopic
 768 composition of the riverine input to the ocean in the correct direction to explain the
 769 trends in all four isotope systems through the late Neogene (Fig. 13). While the
 770 relationships between the different isotope systems discussed here suggest a common
 771 control, the influence of carbonate and dolomite formation on Ca and Mg isotopes are
 772 also likely to have played a significant role in the evolution of these isotope systems
 773 (Tipper et al., 2006b; Fantle and Tipper, 2014). Consequently a future model of
 774 seawater chemistry evolution through the Neogene must also include these additional
 775 factors. Further exploration is also needed to determine the influence of residence
 776 time on the evolution of ocean chemistry. Nonetheless, given the similarities between
 777 the geochemical cycles of B and Li, and despite the large difference in residence time

r.greenop 25/11/2016 13:07

Deleted: four

(Li = 1 million years, B = 11-17 million years), the correlation between these two records is compelling and would no doubt benefit from additional study.

4 Conclusions

Here we present a new $\delta^{11}\text{B}_{\text{sw}}$ record for the Neogene based on paired planktic-benthic $\delta^{11}\text{B}$ measurements. Our new record suggests that $\delta^{11}\text{B}_{\text{sw}}$ (i) was $\sim 37.5\text{‰}$ at the Oligocene-Miocene boundary, (ii) remained low through the middle Miocene, (iii) rapidly increased to the modern value between 12 and 5 Ma, and (iv) plateaued at modern values over the Plio-Pleistocene. Despite some disagreements, [and different uncertainties associated with each approach](#), the fact that our new record, and both of the published data based reconstructions capture the first-order late Miocene $\delta^{11}\text{B}_{\text{sw}}$ rise suggests that consensus is building for the $\delta^{11}\text{B}_{\text{sw}}$ evolution through the Neogene. This emerging view on $\delta^{11}\text{B}_{\text{sw}}$ change provides a vital constraint required to quantitatively reconstruct Neogene ocean pH, ocean carbon chemistry and atmospheric CO_2 using the $\delta^{11}\text{B}$ -pH proxy. When our new $\delta^{11}\text{B}_{\text{sw}}$ record is compared to changes in the seawater isotopic composition of Li, Ca and Mg the shape of the records across the Neogene is remarkably similar. [For all four systems](#), riverine input is cited [a common and key](#) control of the isotopic composition of the [respective](#) elements in seawater. When we compare the isotopic fractionation of the elements associated with secondary mineral formation, the trends in the $\delta^{26}\text{Mg}_{\text{sw}}$, $\delta^{44/40}\text{Ca}_{\text{sw}}$, $\delta^{11}\text{B}_{\text{sw}}$ and $\delta^7\text{Li}_{\text{sw}}$ records are all consistent with an increase in secondary mineral formation through time. While a more quantitative treatment of these multiple stable isotope systems is required, the $\delta^{11}\text{B}_{\text{sw}}$ record presented here provides additional constraints on the processes responsible for the evolution of ocean chemistry through time.

Acknowledgements:

This work used samples provided by (IODP, which is sponsored by the U.S. National Science Foundation and participating countries under the management of Joint Oceanographic Institutions, Inc. We thank W. Hale and A. Wuelbers of the Bremen Core Repository for their kind assistance. The work was supported by NERC

r.greenop 25/11/2016 13:36

Deleted: The increased formation and retention of clays on land may have been related to the growth of the Himalayan orogeny and increased clay formation in the newly formed floodplains and foreland surrounding the mountains (Pogge von Strandmann and Henderson, 2014).

r.greenop 4/12/2016 10:12

Deleted: In all four cases

r.greenop 1/12/2016 18:20

Deleted: as one of the key

grants NE/I006176/1 (G.L.F. and C.H.L.), NE/H006273/1 (G.L.F), NE/I006168/1 and NE/K014137/1 and a Royal Society Research Merit Award (P.A.W), a NERC Independent Research Fellowship NE/K00901X/1 (M.P.H.) and a NERC studentship (R.G). Matthew Cooper, J. Andy Milton, and the B-team are acknowledged for their assistance in the laboratory. [We thank two anonymous reviewers and Philip Pogge von Strandmann for their helpful suggestions that improved the manuscript.](#)

References:

- Al-Rousan, S., Pätzold, J., Al-Moghrabi, S., and Wefer, G., 2004, Invasion of anthropogenic CO₂ recorded in planktonic foraminifera from the northern Gulf of Aqaba: *International Journal of Earth Sciences*, v. 93, no. 6, p. 1066-1076.
- Anagnostou, E., John, E.H., Edgar, K.M., Foster, G.L., Ridgwell, A., Inglis, G.N., Pancost, R.D., Lunt, D.J., Pearson, P.N., 2016, Changing atmospheric CO₂ concentration was the primary driver of early Cenozoic climate, v. 533, p. 380-384.
- Anand, P., Elderfield, H., and Conte, M. H., 2003, Calibration of Mg/Ca thermometry in planktonic foraminifera from a sediment trap time series: *Paleoceanography*, v. 18, no. 2, DOI: 10.1029/2002PA000846.
- Bartoli, G., Hönisch, B., Zeebe, R.E., 2011, Atmospheric CO₂ decline during the Pliocene intensification of Northern Hemisphere glaciations: *Paleoceanography*, v.26, DOI: 10.1029/2010PA002055.
- Badger, M. P. S., Lear, C.H., Pancost, R.D., Foster, G.L., Bailey, T.R., Leng, M.J., and Abels, H.A., 2013, CO₂ drawdown following the middle Miocene expansion of the Antarctic Ice Sheet: *Paleoceanography*, v. 28, doi:10.1002/palo.20015.
- Beerling, D. J., and Royer, D. L., 2011, Convergent Cenozoic CO₂ history: *Nature Geosci*, v. 4, no. 7, p. 418-420.
- Berner, R. A., and Kothavala, Z., 2001, GEOCARB III: A revised model of atmospheric CO₂ over Phanerozoic time: *American Journal of Science*, v. 301, no. 2, p. 182-204.
- Brennan S. T., Lowenstein T. K., Cendón D. I., 2013, The major-ion composition of Cenozoic seawater: the past 36 million years from fluid inclusions in marine halite: *American Journal of Science*, v. 313, p. 713–775.
- Broecker, W. S. and T. H. Peng, 1982, *Tracers in the Sea*, Lamont-Doherty Earth Observatory, Palisades, N. Y.
- Burton, K.W., Vigier, N., 2012, Lithium isotopes as tracers in Marine and terrestrial environments, *Handbook of Environmental Isotope Geochemistry*, Springer, Berlin, Heidelberg, p. 41–59.
- CARINA Group, 2009, Carbon in the Atlantic Ocean Region - the CARINA project: Results and Data, Version 1.0: Carbon Dioxide Information Analysis Center, Oak Ridge National Laboratory, U.S. Department of Energy, Oak Ridge, Tennessee. doi: 10.3334/CDIAC/otg.CARINA.ATL.V1.0

- Catanzaro, E. J., Champion, C., Garner, E., Marinenko, G., Sappenfield, K., and W., S., 1970, Boric Acid: Isotopic and Assay Standard Reference Materials NBS (US) Special Publications. National Bureau of Standards, Institute for Materials Research, Washington, DC.
- Cramer, B., Miller, K., Barrett, P., and Wright, J., 2011, Late Cretaceous-Neogene trends in deep ocean temperature and continental ice volume: Reconciling records of benthic foraminiferal geochemistry ($\delta^{18}\text{O}$ and Mg/Ca) with sea level history: *Journal of Geophysical Research-Oceans*, v. 116, doi:10.1029/2011JC007255.
- Curry W.B. and Oppo D.W., 2005, Glacial water mass geometry and the distribution of $\delta^{13}\text{C}$ of ΣCO_2 in the Western Atlantic Ocean. *Paleoceanography*, v.20, doi:10.1029/2004PA001021
- Delaney, M. L., Be, A. W. H., and Boyle, E. A., 1985, Li, Sr, Mg and Na in foraminiferal calcite shells from laboratory culture, sediment traps and sediment cores: *Geochimica Et Cosmochimica Acta*, v. 49, no. 6, p. 1327-1341.
- Deyhle, A., and Kopf, A., 2004, Possible influence of clay contamination on B isotope geochemistry of carbonaceous samples: *Applied Geochemistry*, v. 19, no. 5, p. 737-745.
- Edwards, N. R. and Marsh, R., 2005, Uncertainties due to transport- parameter sensitivity in an efficient 3-D ocean-climate model: *Clim. Dynam.*, 24, 415–433, doi:10.1007/s00382-004-0508-8.
- Elderfield, H., Yu, J., Anand, P., Kiefer, T., and Nyland, B., 2006, Calibrations for benthic foraminiferal Mg/Ca paleothermometry and the carbonate ion hypothesis: *Earth and Planetary Science Letters*, v. 250, no. 3-4, p. 633-649.
- Evans, D., and Muller, W., 2012, Deep time foraminifera Mg/Ca paleothermometry: Nonlinear correction for secular change in seawater Mg/Ca: *Paleoceanography*, v. 27, DOI: 10.1029/2012PA002315.
- Fantle, M.S., Tipper, E.T., 2014, Calcium isotopes in the global biogeochemical Ca cycle: Implications for development of a Ca isotope proxy, *Earth-Science Reviews*, v. 129, p. 148-177.
- Foster, G., Hönisch, B., Paris, G., Dwyer, G., Rae, J., Elliott, T., Gaillardet, J., Hemming, N., Louvat, P., and Vengosh, A., 2013, Interlaboratory comparison of boron isotope analyses of boric acid, seawater and marine CaCO_3 by MC-ICPMS and NTIMS: *Chemical Geology*, v. 358, p. 1-14.
- Foster, G., Lear, C. H., and Rae, J.W.B., 2012, The evolution of $p\text{CO}_2$, ice volume and climate during the middle Miocene: *Earth and Planetary Science Letters*, v. 341-344, p. 243-254.
- Foster, G. L., 2008, Seawater pH, $p\text{CO}_2$ and $[\text{CO}_3^{2-}]$ variations in the Caribbean Sea over the last 130 kyr: A boron isotope and B/Ca study of planktic foraminifera: *Earth and Planetary Science Letters*, v. 271, no. 1-4, p. 254-266.
- Foster, G. L., Pogge von Strandmann, P. A. E., and Rae, J. W. B., 2010, Boron and magnesium isotopic composition of seawater: *Geochemistry Geophysics Geosystems*, v. 11, DOI: 10.1029/2010GC003201.
- Froelich, F., and Misra, S., 2014. Was the late Paleocene-early Eocene hot because Earth was flat? An ocean lithium isotope view of mountain building, continental weathering, carbon dioxide, and Earth's Cenozoic climate: *Oceanography*, v. 27, no.1, p. 36–49.
- Galbraith, E.D., Kwon, E.Y., Bianchi, D., Hain, M.P., Sarmiento, J.L., 2015, The impact of atmospheric $p\text{CO}_2$ on carbon isotope ratios of the atmosphere and

ocean: *Global Biogeochemical Cycles*, 9, 307–324,
doi:10.1002/2014GB004929

Goodwin, P., and J. M. Lauderdale 2013, Carbonate ion concentrations, ocean carbon storage, and atmospheric CO₂: *Global Biogeochem. Cycles*, 27,
doi:10.1002/gbc.20078.

Gradstein F.M., Ogg J.G., Schmitz M., Ogg G., 2012, *The Geologic Time Scale 2012*: Boston, Elsevier, 1144 p., doi:10.1016/B978-0-444-59425-9.00004-4.

Greenop, R., Foster, G. L., Wilson, P. A., and Lear, C. H., 2014, Middle Miocene climate instability associated with high-amplitude CO₂ variability: *Paleoceanography*, v. 29, no. 9, DOI: 2014PA002653.

Griffith, E., Paytan, A., Caldeira, K., Bullen, T., and Thomas, E., 2008, A Dynamic Marine Calcium Cycle During the Past 28 Million Years: *Science*, v. 322, no. 5908, p. 1671-1674.

Hain, M.P., Sigman, D.M., and Haug, G.H., 2010, Carbon dioxide effects of Antarctic stratification, North Atlantic Intermediate Water formation, and subantarctic nutrient drawdown during the last ice age: Diagnosis and synthesis in a geochemical box model: *Global Biogeochem. Cycles*, v. 24,
doi:10.1029/2010GB003790.

Hain, M.P., Sigman, D.M., and Haug, G.H., 2014a, The Biological Pump in the Past, *Treatise on Geochemistry* 2nd ed., vol. 8, chapter 18, 485-517,
doi:10.1016/B978-0-08-095975-7.00618-5

Hain, M.P., Sigman, D.M., and Haug, G.H., 2014b, Distinct roles of the Southern Ocean and North Atlantic in the deglacial atmospheric radiocarbon decline: *Earth and Planetary Science Letters*, v.394, p.198-208, doi: 10.1016/j.epsl.2014.03.020

Hain, M.P., Sigman, D.M., Higgins, J.A., and Haug, G.H., 2015, The effects of secular calcium and magnesium concentration changes on the thermodynamics of seawater acid/base chemistry: Implications for Eocene and Cretaceous ocean carbon chemistry and buffering: *Global Biogeochem. Cycles*, v. 29, doi:10.1002/2014GB004986.

Hasiuk, F., and Lohmann, K., 2010, Application of calcite Mg partitioning functions to the reconstruction of paleocean Mg/Ca: *Geochimica Et Cosmochimica Acta*, v. 74, no. 23, p. 6751-6763.

Hathorne, E. C., and James, R. H., 2006, Temporal record of lithium in seawater: A tracer for silicate weathering?: *Earth and Planetary Science Letters*, v. 246, no. 3–4, p. 393-406.

Haug, G. H., and Tiedemann, R., 1998, Effect of the formation of the Isthmus of Panama on Atlantic Ocean thermohaline circulation: *Nature*, v. 393, no. 6686, p. 673-676.

Hemleben Ch, Spindler M, Breiting, Ott R., 1987, Morphological and physiological responses of *Globigerinoides sacculifer* (Brady) under varying laboratory conditions: *Marine Micropaleontology*, v.12, p. 305-324.

Hemming, N. G., and Hanson, G. N., 1992, Boron isotopic composition and concentration in modern marine carbonates: *Geochimica et Cosmochimica Acta*, v. 56, no. 1, p. 537-543.

Henehan, M. J., Rae, J. W. B., Foster, G. L., Erez, J., Prentice, K. C., Kucera, M., Bostock, H. C., Martinez-Boti, M. A., Milton, J. A., Wilson, P. A., Marshall, B. J., and Elliott, T., 2013, Calibration of the boron isotope proxy in the planktonic foraminifera *Globigerinoides ruber* for use in palaeo-CO₂ reconstruction: *Earth and Planetary Science Letters*, v. 364, no. 0, p. 111-122.

961 Hindshaw, R. S., Bourdon, B., Pogge von Strandmann, P. A. E., Vigier, N., and
962 Burton, K. W., 2013, The stable calcium isotopic composition of rivers
963 draining basaltic catchments in Iceland: *Earth and Planetary Science Letters*,
964 v. 374, no. 0, p. 173-184.

965 Hodel, D.A., Mueller, P.A., Garrido, J.R., 1991, Variations in the strontium isotopic
966 composition of seawater during the Neogene: *Geology*, v.11, p. 24-27.

967 Holbourn, A., Kuhnt, W., Simo, J., and Li, Q., 2004, Middle Miocene isotope
968 stratigraphy and paleoceanographic evolution of the northwest and southwest
969 Australian margins (Wombat Plateau and Great Australian Bight):
970 *Palaeogeography Palaeoclimatology Palaeoecology*, v. 208, no. 1-2, p. 1-22.

971 Holden, P. B., N. R. Edwards, S. A. Müller, K. I. C. Oliver, R. M. De'ath and A.
972 Ridgwell, 2013. Controls on the spatial distribution of oceanic $\delta^{13}\text{C}_{\text{DIC}}$:
973 *Biogeosciences* 10, 1815-1833.

974 Hönlisch, B., Hemming, N. G., Archer, D., Siddall, M., and McManus, J. F., 2009,
975 Atmospheric Carbon Dioxide Concentration Across the Mid-Pleistocene
976 Transition: *Science*, v. 324, no. 5934, p. 1551-1554.

977 Horita, J., Zimmermann, H., and Holland, H. D., 2002, Chemical evolution of
978 seawater during the Phanerozoic: Implications from the record of marine
979 evaporites: *Geochimica Et Cosmochimica Acta*, v. 66, no. 21, p. 3733-3756.

980 Kaczmarek, K., Nehrke, G., Misra, S., Bijma, J., Elderfield, H., 2016, Investigating
981 the effects of growth rate and temperature on the B/Ca ratio and $\delta^{11}\text{B}$ during
982 inorganic calcite formation, v. 421, p. 81-92.

983 Kakihana, H., Kotaka, M., Satoh, S., Nomura, M., and Okamoto, M., 1977,
984 Fundamental studies on ion-exchange separation of boron isotopes: *Bulletin*
985 *of the Chemical Society of Japan*, v. 50, no. 1, p. 158-163.

986 Keeling, C.D., 1979, The Suess effect: ^{13}C - ^{14}C interrelations: *Environment*
987 *International*, v. 2, no. 4-6, p. 229-300.

988 Key, R. M., Kozyr, A., Sabine, C. L., Lee, K., Wanninkhof, R., Bullister, J. L., Feely,
989 R. A., Millero, F. J., Mordy, C., and Peng, T. H., 2004, A global ocean carbon
990 climatology: Results from Global Data Analysis Project (GLODAP): *Global*
991 *Biogeochem. Cycles*, v. 18, no. 4, doi:10.1029/2004GB002247.

992 Kısakürek, B., James, R. H., and Harris, N. B. W., 2005, Li and $\delta^7\text{Li}$ in Himalayan
993 rivers: Proxies for silicate weathering?: *Earth and Planetary Science Letters*,
994 v. 237, no. 3-4, p. 387-401.

995 Klochko, K., Kaufman, A. J., Yao, W. S., Byrne, R. H., and Tossell, J. A., 2006,
996 Experimental measurement of boron isotope fractionation in seawater: *Earth*
997 *and Planetary Science Letters*, v. 248, no. 1-2, p. 276-285.

998 Lear, C. H., Mawbey, E. M., and Rosenthal, Y., 2010, Cenozoic benthic foraminiferal
999 Mg/Ca and Li/Ca records: Toward unlocking temperatures and saturation
1000 states: *Paleoceanography*, v. 25, doi:10.1029/2009PA001880.

1001 Lee, K., Kim, T. W., Byrne, R. H., Millero, F. J., Feely, R. A., and Liu, Y. M., 2010,
1002 The universal ratio of boron to chlorinity for the North Pacific and North
1003 Atlantic oceans: *Geochimica Et Cosmochimica Acta*, v. 74, no. 6, p. 1801-
1004 1811.

1005 Lemarchand, D., and Gaillardet, J., 2006, Transient features of the erosion of shales
1006 in the Mackenzie basin (Canada), evidences from boron isotopes: *Earth and*
1007 *Planetary Science Letters*, v. 245, no. 1-2, p. 174-189.

1008 Lemarchand, D., Gaillardet, J., Lewin, E., and Allegre, C. J., 2000, The influence of
1009 rivers on marine boron isotopes and implications for reconstructing past ocean
1010 pH: *Nature*, v. 408, p. 951-954.

- Li, G.-J. and West, A.J., 2014, Evolution of Cenozoic seawater lithium isotopes: coupling of global denudation regime and shifting seawater sinks: *Earth Planet. Sci. Lett.*, v. 401, p. 284-293.
- Liu, W. G., Xiao, Y. K., Peng, Z. C., An, Z. S., and He, X. X., 2000, Boron concentration and isotopic composition of halite from experiments and salt lakes in the Qaidam Basin: *Geochimica Et Cosmochimica Acta*, v. 64, no. 13, p. 2177-2183.
- Liu, X.-M., Wanner, C., Rudnick, R. L., and McDonough, W. F., 2015, Processes controlling $\delta^7\text{Li}$ in rivers illuminated by study of streams and groundwaters draining basalts: *Earth and Planetary Science Letters*, v. 409, no. 0, p. 212-224.
- Lynch-Steiglitz, J., T.F. Stocker, W.S. Broecker and R.G. Fairbanks (1995), The influence of air-sea exchange on the isotopic composition of oceanic carbon: Observations and modeling: *Global Biogeochemical Cycles*, vol. 9, 4, p653-665.
- Martinez-Boti, M. A., Foster, G. L., Chalk, T. B., Rohling, E. J., Sexton, P. F., Lunt, D. J., Pancost, R. D., Badger, M. P. S., and Schmidt, D. N., 2015a, Pliocene Pleistocene climate sensitivity from on a new high-resolution CO_2 record: *Nature*, v. 518, p. 49-54.
- Martinez-Boti, M.A., Marino, G., Foster, G. L., Ziveri, P., Henahan, M. J., Rae, J. W. B., Mortyn, P. G. and Vance, D., 2015b, Boron isotope evidence for oceanic CO_2 leakage during the last deglaciation: *Nature*, v. 518, p. 219-222.
- McCorkle, D. C., Corliss, B. H., and Farnham, C. A., 1997, Vertical distributions and stable isotopic compositions of live (stained) benthic foraminifera from the North Carolina and California continental margins: *Deep Sea Research Part I: Oceanographic Research Papers*, v. 44, no. 6, p. 983-1024.
- Millot, R., Vigier, N., and Gaillardet, J., 2010, Behaviour of lithium and its isotopes during weathering in the Mackenzie Basin, Canada: *Geochimica et Cosmochimica Acta*, v. 74, no. 14, p. 3897-3912.
- Misra, S., and Froelich, P., 2012, Lithium Isotope History of Cenozoic Seawater: Changes in Silicate Weathering and Reverse Weathering: *Science*, v. 335, no. 6070, p. 818-823.
- Ockert, C., Gussone, N., Kaufhold, S., Teichert, B.M.A., 2013, Isotope fractionation during Ca exchange on clay minerals in a marine environment: *Geochimica et Cosmochimica Acta*, v. 112, p. 374-388.
- Olsen, A., Ninneman, U.S., 2010, Large $\delta^{13}\text{C}$ gradients in the preindustrial North Atlantic revealed: *Science*, v. 330, p. 658-659.
- Pälike, H., Lyle, M., Nishi, H., Raffi, I., Ridgwell, A., Gamage, K., Klaus, A., Acton, G., Anderson, L., Backman, J., Baldauf, J., Beltran, C., *et al.* 2012, A Cenozoic record of the equatorial Pacific carbonate compensation depth: *Nature*, v. 488, no. 7413, p. 609-614.
- Palmer, M. R., Pearson, P. N., and Cobb, S. J., 1998, Reconstructing past ocean pH-depth profiles: *Science*, v. 282, no. 5393, p. 1468-1471.
- Paris, G., Gaillardet, J., and Louvat, P., 2010, Geological evolution of seawater boron isotopic composition recorded in evaporites: *Geology*, v. 38, no. 11, p. 1035-1038.
- Park, H., and Schlesinger, W. H., 2002, Global biogeochemical cycle of boron: *Global Biogeochemical Cycles*, v. 16, no. 4, DOI: 10.1029/2001GB001766.

- 1059 Pearson, P. N., Foster, G. L., and Wade, B. S., 2009, Atmospheric carbon dioxide
1060 through the Eocene-Oligocene climate transition: *Nature*, v. 461, p. 1110-
1061 1113.
- 1062 Pearson, P. N., and Wade, B. S., 2009, Taxonomy and Stable Isotope Paleocology of
1063 Well-Preserved Planktonic Foraminifera from the Uppermost Oligocene of
1064 Trinidad: *Journal of Foraminiferal Research*, v. 39, no. 3, p. 191-217.
- 1065 Pearson, P. N., and Palmer, M. R., 1999, Middle Eocene seawater pH and
1066 atmospheric carbon dioxide concentrations: *Science*, v. 284, no. 5421, p.
1067 1824-1826.
- 1068 Pearson, P. N., and Palmer, M. R., 2000, Atmospheric carbon dioxide concentrations
1069 over the past 60 million years: *Nature*, v. 406, no. 6797, p. 695-699.
- 1070 Pistiner, J. S., and Henderson, G. M., 2003, Lithium-isotope fractionation during
1071 continental weathering processes: *Earth and Planetary Science Letters*, v. 214,
1072 no. 1-2, p. 327-339.
- 1073 Pogge von Strandmann, P. A. E., Burton, K. W., James, R. H., van Calsteren, P.,
1074 Gislason, S. R., and Sigfússon, B., 2008, The influence of weathering
1075 processes on riverine magnesium isotopes in a basaltic terrain: *Earth and*
1076 *Planetary Science Letters*, v. 276, no. 1-2, p. 187-197.
- 1077 Pogge von Strandmann, P. A. E., Forshaw, J., and Schmidt, D. N., 2014, Modern and
1078 Cenozoic records of seawater magnesium from foraminiferal Mg isotopes:
1079 *Biogeosciences*, v. 11, no. 18, p. 5155-5168.
- 1080 Pogge von Strandmann, P. A. E., and Henderson, G. M., 2014, The Li isotope
1081 response to mountain uplift: *Geology*, doi: 10.1130/G36162.1.
- 1082 Rae, J. W. B., Foster, G. L., Schmidt, D. N., and Elliott, T., 2011, Boron isotopes and
1083 B/Ca in benthic foraminifera: Proxies for the deep ocean carbonate system:
1084 *Earth and Planetary Science Letters*, v. 302, no. 3-4, p. 403-413.
- 1085 Raitzsch, M., and Hönisch, B., 2013, Cenozoic boron isotope variations in benthic
1086 foraminifers: *Geology*, v. 41, no. 5, p. 591-594.
- 1087 Ridgwell, A., 2005, A mid Mesozoic revolution in the regulation of ocean
1088 chemistry: *Marine Geology*, v. 217, no. 3-4, p. 339-357.
- 1089 Ridgwell, A., Hargreaves, J. C., Edwards, N. R., Annan, J. D., Lenton, T. M., Marsh,
1090 R., Yool, A., and Watson, A., 2007, Marine geo-chemical data assimilation in
1091 an efficient Earth System Model of global biogeochemical cycling:
1092 *Biogeosciences*, 4, 87-104, doi:10.5194/bg-4-87-2007, 2007.
- 1093 Rose, E. F., Chaussidon, M., and France-Lanord, C., 2000, Fractionation of boron
1094 isotopes during erosion processes: the example of Himalayan rivers:
1095 *Geochimica et Cosmochimica Acta*, v. 64, no. 3, p. 397-408.
- 1096 Rose-Koga, E. F., Sheppard, S. M. F., Chaussidon, M., and Carignan, J., 2006, Boron
1097 isotopic composition of atmospheric precipitations and liquid-vapour
1098 fractionations: *Geochimica et Cosmochimica Acta*, v. 70, no. 7, p. 1603-1615.
- 1099 Sanyal, A., Hemming, N.G., Hanson, G.N., Broecker, W.S., 1995, Evidence for a
1100 higher pH in the glacial ocean from boron isotopes in foraminifera: *Nature*,
1101 373, p. 243-236
- 1102 Sanyal, A., Bijma, J., Spero, H., and Lea, D. W., 2001, Empirical relationship
1103 between pH and the boron isotopic composition of *Globigerinoides sacculifer*:
1104 Implications for the boron isotope paleo-pH proxy: *Paleoceanography*, v. 16,
1105 no. 5, p. 515-519.
- 1106 Schlitzer, R., Ocean Data View, 2016, <http://www.awi-bremerhaven.de/GEO/ODV>.

1107 Seki, O., Foster, G. L., Schmidt, D. N., Mackensen, A., Kawamura, K., and Pancost,
 1108 R. D., 2010, Alkenone and boron-based Pliocene $p\text{CO}_2$ records: Earth and
 1109 Planetary Science Letters, v. 292, no. 1-2, p. 201-211.
 1110 Shipboard Scientific Party, 1989. Site 758. In Peirce, J., Weissel, J., et al., *Proc.*
 1111 *ODP, Init. Repts.*, 121: College Station, TX (Ocean Drilling Program), 359–
 1112 453. doi:10.2973/odp.proc.ir.121.112.1989
 1113 Shipboard Scientific Party, 1995. Site 926. In Curry, W.B., Shackleton, N.J., Richter,
 1114 C., et al., *Proc. ODP, Init. Repts.*, 154: College Station, TX (Ocean Drilling
 1115 Program), 153–232. doi:10.2973/odp.proc.ir.154.105.1995
 1116 Shipboard Scientific Party, 1997. Site 999. In Sigurdsson, H., Leckie, R.M., Acton,
 1117 G.D., et al., *Proc. ODP, Init. Repts.*, 165: College Station, TX (Ocean Drilling
 1118 Program), 131–230. doi:10.2973/odp.proc.ir.165.104.1997.
 1119 Sigman, D.M., McCorkle, D.C., Martin, W.R., 1998, The calcite lysocline as a
 1120 constraint on glacial/interglacial low-latitude production changes: Global
 1121 Biogeochem. Cycles, v. 12, no. 3, p. 409-427.
 1122 Simon, L., Lecuyer, C., Marechal, C., and Coltice, N., 2006, Modelling the
 1123 geochemical cycle of boron: Implications for the long-term $\delta^{11}\text{B}$ evolution of
 1124 seawater and oceanic crust: Chemical Geology, v. 225, no. 1-2, p. 61-76.
 1125 Smith, H. J., Spivack, A. J., Staudigel, H., and Hart, S. R., 1995, The boron isotopic
 1126 composition of altered oceanic crust: Chemical Geology, v. 126, no. 2, p. 119-
 1127 135.
 1128 | Spero, H., Mielke, K., Kalve, E., Lea, D., and Pak, D., 2003, Multispecies approach
 1129 to reconstructing eastern equatorial Pacific thermocline hydrography during
 1130 the past 360 kyr: Paleoceanography, v. 18, no. 1,
 1131 doi:10.1029/2001GC000200.
 1132 Spezzaferri S, Kucera M, Pearson PN, Wade BS, Rappo S, Poole CR, et al., 2015,
 1133 Fossil and genetic evidence for the polyphyletic nature of the planktonic
 1134 foraminifera "*Globigerinoides*", and description of the new Genus *Trilobatus*:
 1135 PLoS ONE, v.10, no. 5, DOI:e0128108. doi:10.1371/journal.pone.0128108
 1136 Spivack, A. J., and Edmond, J. M., 1987, Boron isotope exchange between seawater
 1137 and the oceanic crust: Geochimica et Cosmochimica Acta, v. 51, no. 5, p.
 1138 1033-1043.
 1139 Takahashi, T., Sutherland S.C., Wanninkhof, R., Sweeney, C., Feely, R.A., et al.,
 1140 2009, Climatological mean and decadal change in surface ocean $p\text{CO}_2$, and
 1141 net sea-air CO_2 flux over global oceans: Deep-Sea Research II, v.56, p.554-
 1142 557.
 1143 Tipper, E. T., Galy, A., and Bickle, M. J., 2006a, Riverine evidence for a fractionated
 1144 reservoir of Ca and Mg on the continents: Implications for the oceanic Ca
 1145 cycle: Earth and Planetary Science Letters, v. 247, no. 3–4, p. 267-279.
 1146 Tipper, E. T., Galy, A., Gaillardet, J., Bickle, M. J., Elderfield, H., and Carder, E. A.,
 1147 2006b, The magnesium isotope budget of the modern ocean: Constraints from
 1148 riverine magnesium isotope ratios: Earth and Planetary Science Letters, v.
 1149 250, no. 1–2, p. 241-253.
 1150 Tomascak, P. B., 2004, Developments in the Understanding and Application of
 1151 Lithium Isotopes in the Earth and Planetary Sciences: Reviews in Mineralogy
 1152 and Geochemistry, v. 55, no. 1, p. 153-195.
 1153 Tyrrell, T., and Zeebe, R. E., 2004, History of carbonate ion concentration over the
 1154 last 100 million years: Geochimica Et Cosmochimica Acta, v. 68, no. 17, p.
 1155 3521-3530.

r.greenop 1/12/2016 17:40

Deleted: Sosdian, S.M., Greenop, R.,
 Lear, C.H., Foster, G.L., Hain, M.P., and
 Pearson, P.N., 2015, Future ocean
 acidification could be unprecedented in the
 last 14 million years: in prep. -

- Vengosh, A., Starinsky, A., Kolodny, Y., Chivas, A. R., and Raab, M., 1992, Boron Isotope Variations during Fractional Evaporation of Sea-Water - New Constraints on the Marine Vs Nonmarine Debate: *Geology*, v. 20, no. 9, p. 799-802.
- [Vigier, N., Godd  ris, Y., 2015, A new approach for modeling Cenozoic oceanic lithium isotope paleo-variations: the key role of climate: *Climate of the Past*, v.11, p.635-645.](#)
- [Wanner, C., Sonnenthal, E. L., and Liu, X.-M., 2014, Seawater \$\delta^7\text{Li}\$: a direct proxy for global \$\text{CO}_2\$ consumption by continental silicate weathering?: *Chem. Geol.*, 154-167.](#)
- Wimpenny, J., Colla, C. A., Yin, Q.-Z., Rustad, J. R., and Casey, W. H., 2014, Investigating the behaviour of Mg isotopes during the formation of clay minerals: *Geochimica et Cosmochimica Acta*, v. 128, no. 0, p. 178-194.
- Wombacher, F., Eisenhauer, A., B  hm, F., Gussone, N., Regenberg, M., Dullo, W. C., and R  ggeberg, A., 2011, Magnesium stable isotope fractionation in marine biogenic calcite and aragonite: *Geochimica et Cosmochimica Acta*, v. 75, no. 19, p. 5797-5818.
- You, C.F., Spivack, A. J., Smith, J. H., and Gieskes, J. M., 1993, Mobilization of boron in convergent margins: Implications for the boron geochemical cycle: *Geology*, v. 21, no. 3, p. 207-210.
- Zeebe, R. E., and Wolf-Gladrow, D. A., 2001, *CO_2 in seawater, equilibrium, kinetics, isotopes* IN Elsevier oceanography series, Amsterdam, PAYS-BAS, Elsevier, XIII, 346 p. p.:
- Zeeden, C., Hilgen, F., Westerhold, T., Lourens, L., R  hl, U., and Bickert, T., 2013, Revised Miocene splice, astronomical tuning and calcareous plankton biochronology of ODP Site 926 between 5 and 14.4 Ma: *Palaeogeography, Palaeoclimatology, Palaeoecology*, v. 369, no. 0, p. 430-451.

Figure Captions:

Figure 1: The oceanic boron cycle. Fluxes are from Lemarchand et al. (2000) and Park and Schlesinger (2002). Isotopic compositions are from Lemarchand et al. (2000), Foster et al., (2010) and references therein.

Figure 2: A compilation of published $\delta^{11}\text{B}_{\text{sw}}$ records. Seawater composition reconstructed from foraminifera depth profiles (light blue squares and dark blue cross) from Pearson and Palmer (2000) and Foster et al. (2012) respectively, numerical modelling (green line), with additional green lines shows $\pm 1 \text{ ‰}$ confidence interval (Lemarchand et al., 2000), benthic $\delta^{11}\text{B}$ (purple diamonds and dark purple line [showing 5pt moving average](#) is using the fractionation factor of Klochko et al., 2006, light purple line [showing 5pt moving average](#) using an empirical calibration) from Raitzsch and H  nisch (2013), and halites (orange crosses)

from Paris et al. (2010). The orange crosses in brackets were discarded from the original study.

Figure 3: Schematic diagram showing the change in pH gradient with a 3‰ change in $\delta^{11}\text{B}$ for $\delta^{11}\text{B}_{\text{sw}}$ of a) 39.6‰ and b) 37.5‰. Arrows highlight the different pH gradients. Note how a $\delta^{11}\text{B}$ difference of 3 ‰ is translated into different pH gradients depending on the $\delta^{11}\text{B}_{\text{sw}}$. Calculated using $B_T = 432.6 \mu\text{mol/kg}$ (Lee et al., 2010) and $\alpha_B = 1.0272$ (Klochko et al., 2006). (c) The pH change for a $\delta^{11}\text{B}$ change of 3 ‰ at a range of different $\delta^{11}\text{B}_{\text{sw}}$.

Figure 4: Map of study sites and mean annual air-sea disequilibria with respect to $p\text{CO}_2$. The black dots indicate the location of the sites used in this study. ODP Sites 758, 999, 926 and 761 used in this study are highlighted with water depth. Data are from (Takahashi et al., 2009) plotted using ODV (Schlitzer, 2016).

Figure 5: Latitudinal cross-section through the Atlantic showing (a) pH variations; (b) the $\delta^{13}\text{C}$ composition. Data are plotted using Ocean Data View (Schlitzer 2016). pH data are from the CARINA dataset (CARINA group, 2009) and the $\delta^{13}\text{C}$ data are from the GLODAP data compilation (Key et al., 2004); (c) pH and $\delta^{13}\text{C}_{\text{DIC}}$ relationships in the modern ocean adapted from Foster et al., (2012). [Data are from all the ocean basins spanning approximately 40°N to 40°S.](#) Because of anthropogenic acidification and the Suess effect only data from >1500 m are plotted. Also included in the plot are the data from a transect in the North Atlantic (from 0 to 5000 m) where the effects of anthropogenic perturbation on both parameters have been corrected (Olsen and Ninneman, 2010).

Figure 6: $\delta^{11}\text{B}_{\text{planktic}}$, temperature and $\delta^{13}\text{C}_{\text{DIC}}$ estimates for the surface and deep ocean through the last 23 million years. (a) $\delta^{11}\text{B}_{\text{planktic}}$ surface; (b) $\delta^{11}\text{B}_{\text{borate}}$ deep from benthic foraminifera (blue) from this study and (green) Raitzsch and Hönisch, (2013). The error bars show the analytical external reproducibility at 95% confidence [for this study. For the Raitzsch & Hönisch \(2013\) data the error bars represent propagated uncertainties of external reproducibilities of time equivalent benthic foraminifer samples from different core sites in different ocean basins](#); (c) Mg/Ca based temperature reconstructions of surface dwelling planktic foraminifera; (d) Deep water temperature estimates from Cramer et al. (2011); (e) $\delta^{13}\text{C}_{\text{DIC}}$ surface record; (f) $\delta^{13}\text{C}_{\text{DIC}}$ benthic record. Squares depict ODP Site 999, triangles are ODP Site 758,

diamonds are ODP Site 926, circles are ODP Site 761. Species are highlighted by colour: Orange are *T. trilobus*, purple *G. ruber*, pink *G. praebulloides*, dark blue *Cibicidoides wuellerstorfi* and light blue *Cibicidoides mundulus*. The two benthic-planktic pairs that were removed prior to smoothing are highlighted with arrows.

Figure 7: The output from GENIE sensitivity analysis showing the warm-surface-to-cold-deep ΔpH -to- $\Delta\delta^{13}\text{C}$ relationship. A pre-industrial model setup was taken and perturbations were made to alkalinity inventory, carbon inventory, Antarctic shelf fresh water flux (Sv), Atlantic-Pacific freshwater flux, S. Lim gas exchange (blocks air-sea gas exchange south of the stated latitude), remineralisation depth scale (m) and rain ratio – as described in the methods section. Blue circles depict the ΔpH -to- $\Delta\delta^{13}\text{C}$ relationship (where the colours reflect the CO_2 level of each experiment) and red open circles show the root mean square of the regression (RMSE). The green stars are the ΔpH -to- $\Delta\delta^{13}\text{C}$ relationship for the control experiment conducted at 292.67 ppm CO_2 . The green (open) points show the RMSE for this control run. Inventories are dimensionless (1 is control). For the Atlantic-Pacific FWF 1 is equivalent to 0.32 Sv. The alkalinity and carbon inventory experiments are very extreme and inconsistent with geologic evidence.

Figure 8: The output from sensitivity analysis of the relationship between pH gradient and $\delta^{13}\text{C}$ gradient from the 13500 run CYCLOPS ensemble (see text for model details). Panel (a) shows the mean gradient when the result from all 18 ocean boxes are included in the regression. Panel (b) shows only the boxes from the low latitude ocean from all basins and (c) shows the regression from only North Atlantic low latitude boxes. Note the lower $\Delta\text{pH}/\Delta\delta^{11}\text{B}$ slope at the lower latitudes due to the effect of temperature. The 0.201 line in each panel is the mean gradient when all the ocean boxes are included in the regression.

Figure 9: The pH gradient between surface and deep through time calculated from the $\delta^{13}\text{C}$ gradient and using a flat probability derived from the low latitude ensemble regressions from the CYCLOPS model. The modern pH gradients at each site are also plotted.

Figure 10: The calculated $\delta^{11}\text{B}_{\text{sw}}$ from the benthic-planktic $\delta^{11}\text{B}$ pairs using a pH gradient derived from $\delta^{13}\text{C}$. The uncertainty on each data point is determined using a Monte Carlo approach including uncertainties in temperature, salinity, $\delta^{11}\text{B}$ and the

r.greenop 25/11/2016 16:37

Deleted: red

r.greenop 25/11/2016 14:18

Deleted: wuellerstorfi

r.greenop 25/11/2016 14:47

Formatted: Font:14 pt, Not Italic

1268 pH gradient (see text for details). Data are plotted as box and whisker diagrams
 1269 where the median and interquartile range as plotted in the box and whiskers show the
 1270 maximum and minimum output from the Monte Carlo simulations. The line of best
 1271 fit is the probability maximum of a LOWESS fit given the uncertainty in the
 1272 calculated $\delta^{11}\text{B}_{\text{sw}}$. The darker shaded area highlights the 68% confidence interval and
 1273 the lighter interval highlights the 95% confidence interval. The bottom panel shows
 1274 box plots of the mean and 2 standard error (s.e.) of 'binning' the individual $\delta^{11}\text{B}_{\text{sw}}$
 1275 measurements into 8 Myr intervals. The middle line is the mean and the box shows
 1276 the 2 s.e. of the data points in that bin. The smoothed record is also plotted for
 1277 comparison where the line of best fit is the probability maximum of a LOWESS fit
 1278 given the uncertainty in the calculated $\delta^{11}\text{B}_{\text{sw}}$. The darker shaded area highlights the
 1279 68% confidence interval and the lighter interval highlights the 95% confidence
 1280 interval. The black dot is the modern value of 39.61 ‰ (Foster et al., 2010).

1281 Figure 11: The $\delta^{11}\text{B}_{\text{sw}}$ curve calculated using the variable pH gradient derived from
 1282 $\delta^{13}\text{C}$. The median (red line), 68% (dark red band) and 95% (light red band)
 1283 confidence intervals are plotted. Plotted with a compilation of published $\delta^{11}\text{B}_{\text{sw}}$
 1284 records. Seawater composition reconstructed from foraminifera depth profiles (light
 1285 blue squares and dark blue cross) from Pearson and Palmer (2000) and Foster et al.
 1286 (2012) respectively, numerical modelling (green line), with additional green lines
 1287 shows ± 1 ‰ confidence interval (Lemarchand et al., 2000) and benthic $\delta^{11}\text{B}$ (purple
 1288 diamonds and dark purple line [showing 5pt moving average](#) is using the fractionation
 1289 factor of Klochko et al., 2006, light purple line [showing 5pt moving average](#) using an
 1290 empirical calibration) from Raitzsch and Hönisch (2013). All the published $\delta^{11}\text{B}_{\text{sw}}$
 1291 curves are adjusted so that at $t=0$, the isotopic composition is equal to the modern
 1292 (39.61 ‰).

1293 Figure 12: a) The $\delta^{11}\text{B}_{\text{sw}}$ curve from this study plotted with other trace element
 1294 isotopic records. On the $\delta^{11}\text{B}_{\text{sw}}$ panel the darker shaded area highlights the 68%
 1295 confidence interval and the lighter interval highlights the 95% confidence interval),
 1296 $\delta^{26}\text{Mg}_{\text{sw}}$ record from Pogge von Strandmann et al. (2014) (error bars are ± 0.28 ‰
 1297 and include analytical uncertainty and scatter due to the spread in modern *O. universa*
 1298 and the offset between the two analysed species), $\delta^{44/40}\text{Ca}_{\text{sw}}$ record from Griffith et al.
 1299 (2008) (error bars show 2σ uncertainty) and $\delta^7\text{Li}_{\text{sw}}$ record from Misra and Froelich

r.greenop 4/12/2016 10:56

Deleted: green

1301 (2012) (error bars show 2 σ uncertainty). Blue dashed lines show middle Miocene
1302 values, red dashed lines highlight the modern.

1303 | Figure 13: Crossplots of the records of $\delta^{11}\text{B}_{\text{sw}}$ using a variable pH gradient derived
1304 from $\delta^{13}\text{C}$ (error bars show 2 σ uncertainty) with $\delta^{44/40}\text{Ca}_{\text{sw}}$ from Griffith et al. (2008)
1305 (error bars show 2 σ uncertainty), $\delta^7\text{Li}_{\text{sw}}$ from Misra and Froelich (2012) (error bars
1306 show 2 σ uncertainty) and $\delta^{26}\text{Mg}_{\text{sw}}$ from Pogge von Strandmann et al. (2014) (error
1307 bars are ± 0.28 ‰ and include analytical uncertainty and scatter due to the spread in
1308 modern *O. universa* and the offset between the two analysed species). The colour of
1309 the data points highlights the age of the data points where red = modern and blue =
1310 23 Ma.

1311 Table 1: CYCLOPS model parameter values defining the ensemble of 13,500
1312 simulations.

1313 Table 2: Uncertainty inputs into the Monte Carlo simulations to calculate $\delta^{11}\text{B}$. The
1314 sources of uncertainty are also added. All uncertainty estimates are 2 σ .

1315 Table 3: The average $\delta^{11}\text{B}$, $\delta^{26}\text{Mg}$, $\delta^{44/40}\text{Ca}$ and $\delta^7\text{Li}$ composition of major fluxes into
1316 and out of the ocean. Colour coding reflects the relative importance of each the
1317 processes (darker shading reflects greater importance). The colour coding for boron is
1318 based on Lemarchand et al. (2000) and references therein, lithium from Misra and
1319 Froelich (2012) and references therein, magnesium from Tipper et al. (2006b) and
1320 calcium from Fantle and Tipper (2014) and Griffin et al. (2008) and references
1321 therein. The isotopic ratio of each process is: (a) Lemarchand et al. (2000) and
1322 references therein; b) Misra and Froelich (2012) and references therein; (c) Burton
1323 and Vigier (2012); (d) Tipper et al. (2006b); e) Wombacher et al. (2011); f) includes
1324 dolomitisation; g) removal through hydrothermal activity; h) Griffith et al. (2008); i)
1325 Fantle and Tipper (2014) and references therein; j) dolomitisation may be an
1326 important component of the carbonate flux. Modern $\delta^{26}\text{Mg}_{\text{sw}}$ and $\delta^{11}\text{B}_{\text{sw}}$ from Foster
1327 et al. (2010), $\delta^7\text{Li}_{\text{sw}}$ from Tomascak (2004). The $\delta^{44/40}\text{Ca}$ presented here was
1328 measured relative to seawater and hence seawater has a $\delta^{44/40}\text{Ca}_{\text{sw}}$ of 0 permil by
1329 definition.

1330

r.greenop 4/12/2016 10:58

Deleted: the

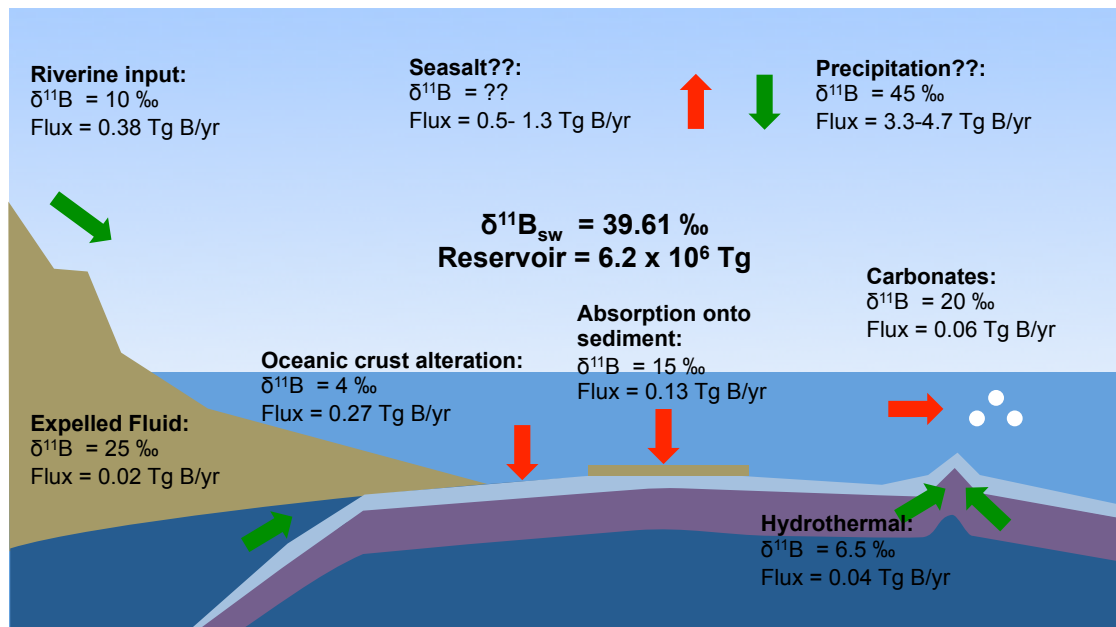
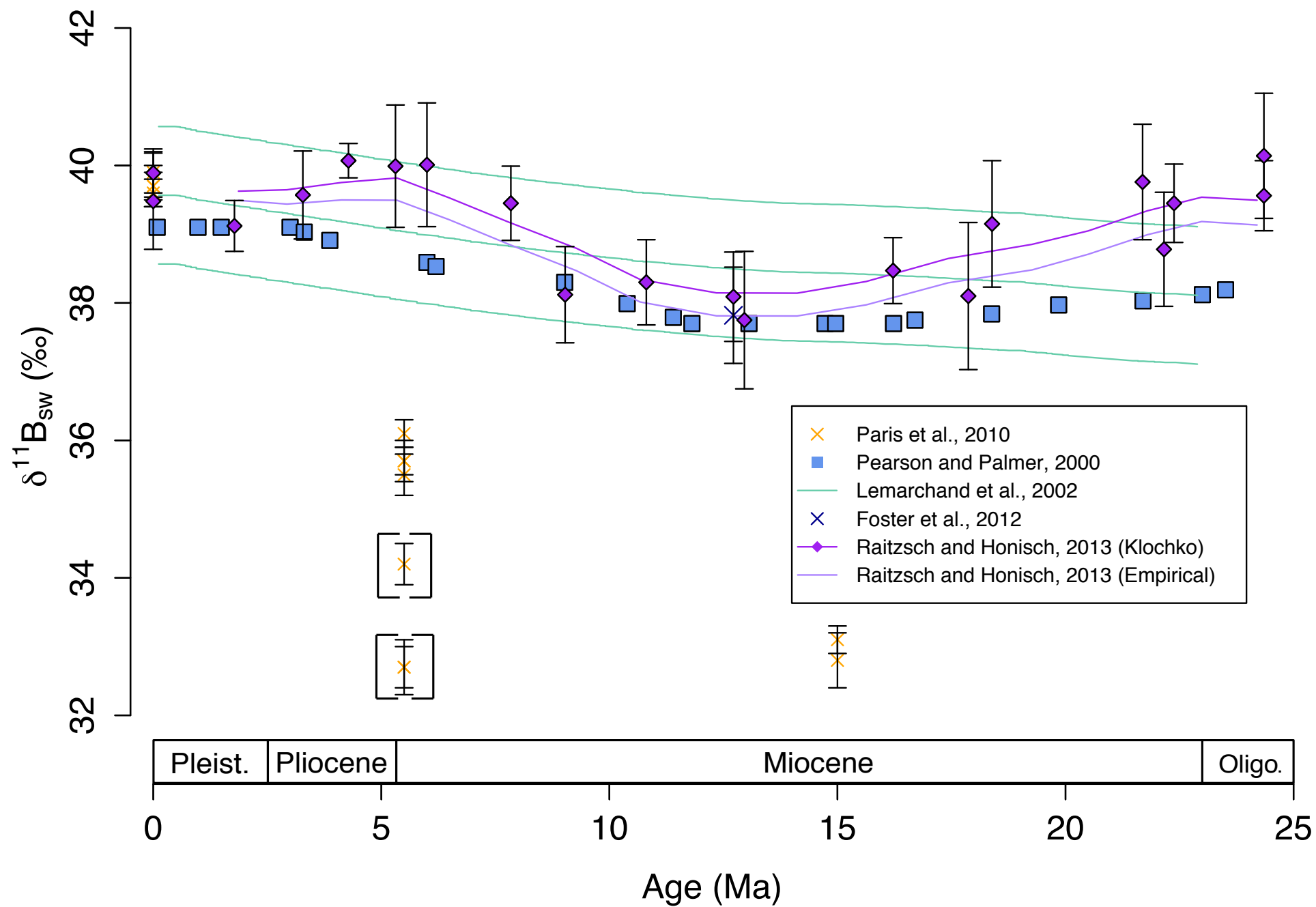


Figure 1

Figure 2



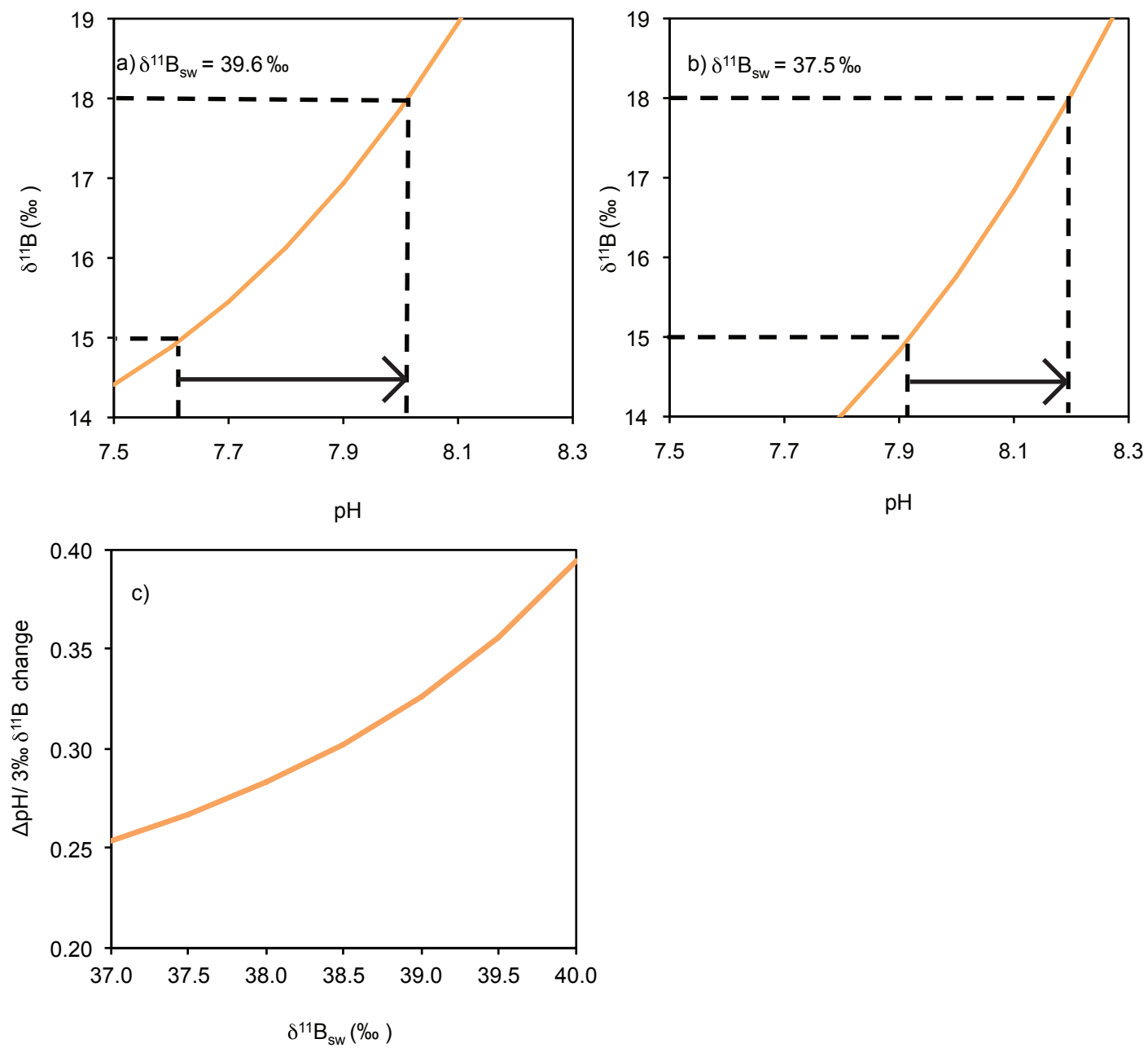


Figure 3

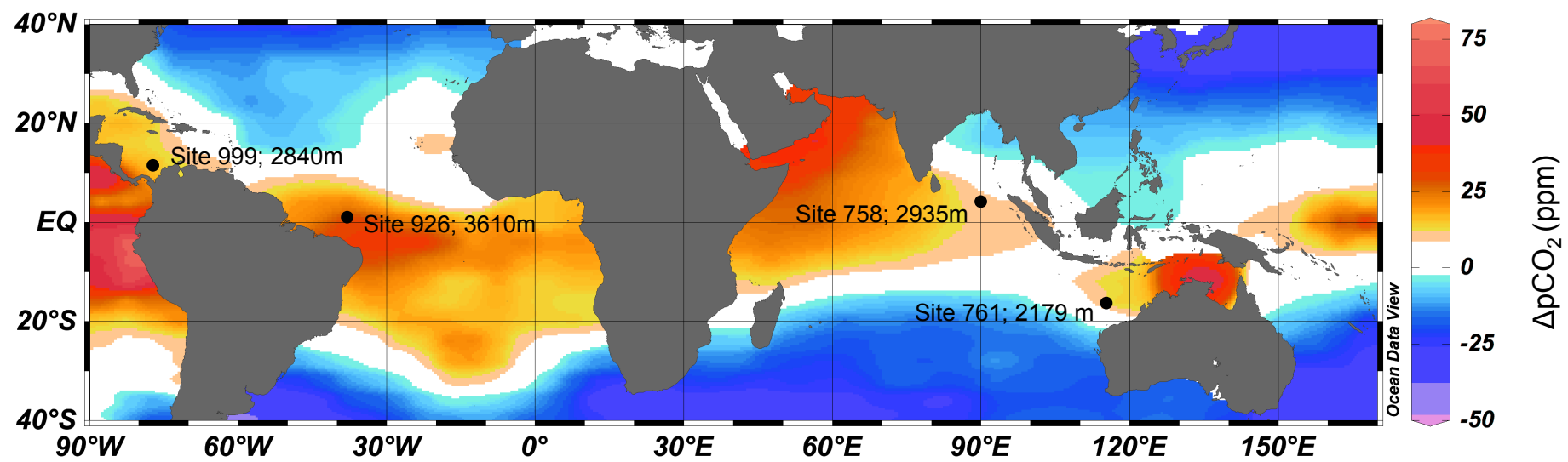


Figure 4

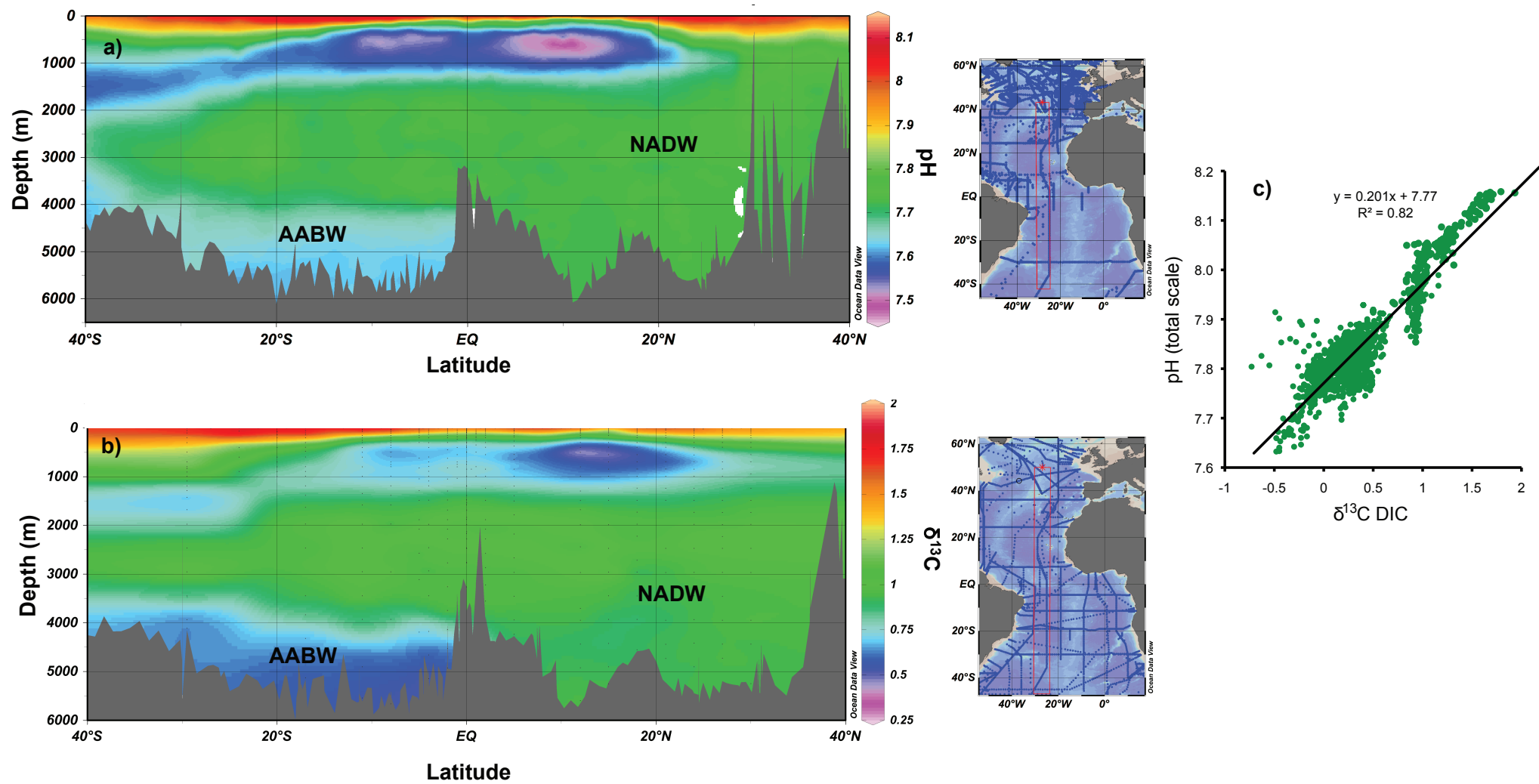
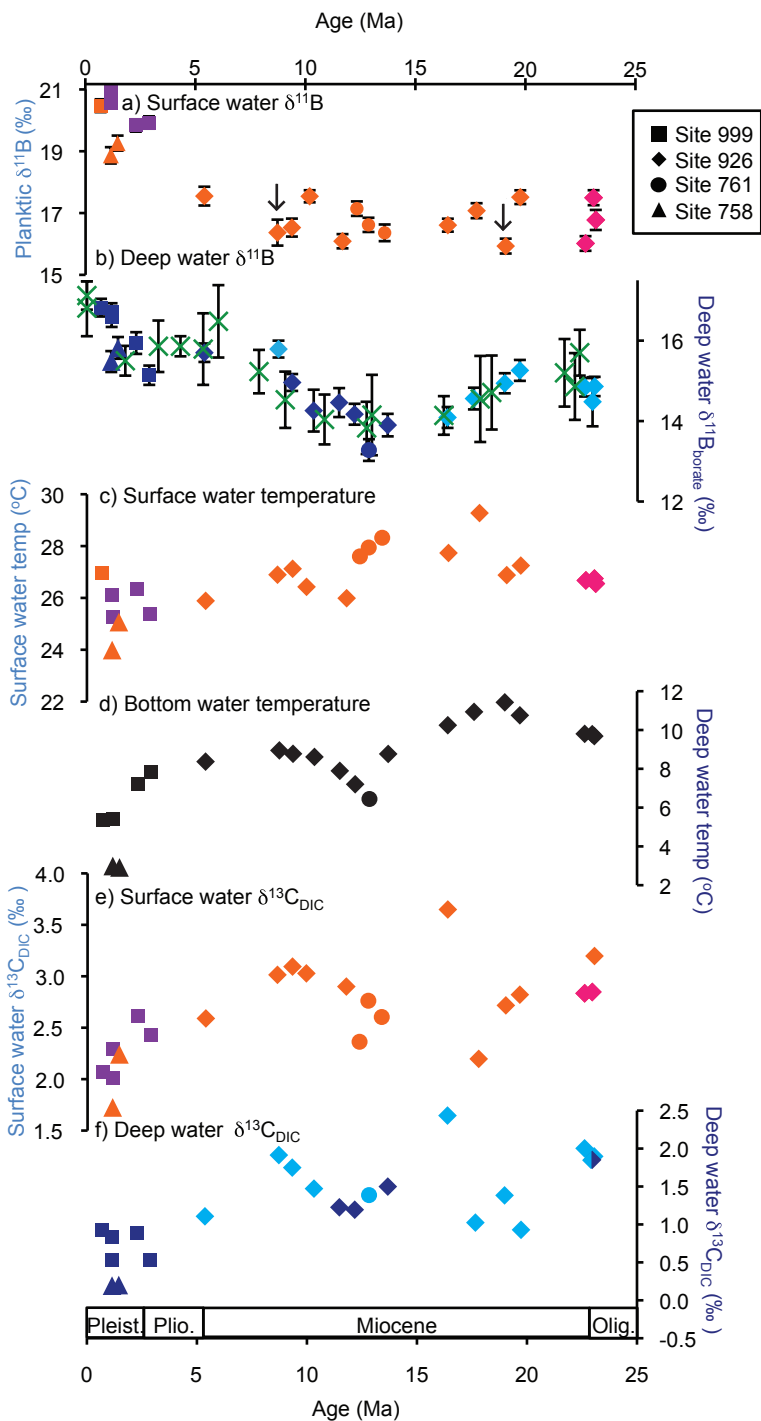


Figure 5

Figure 6



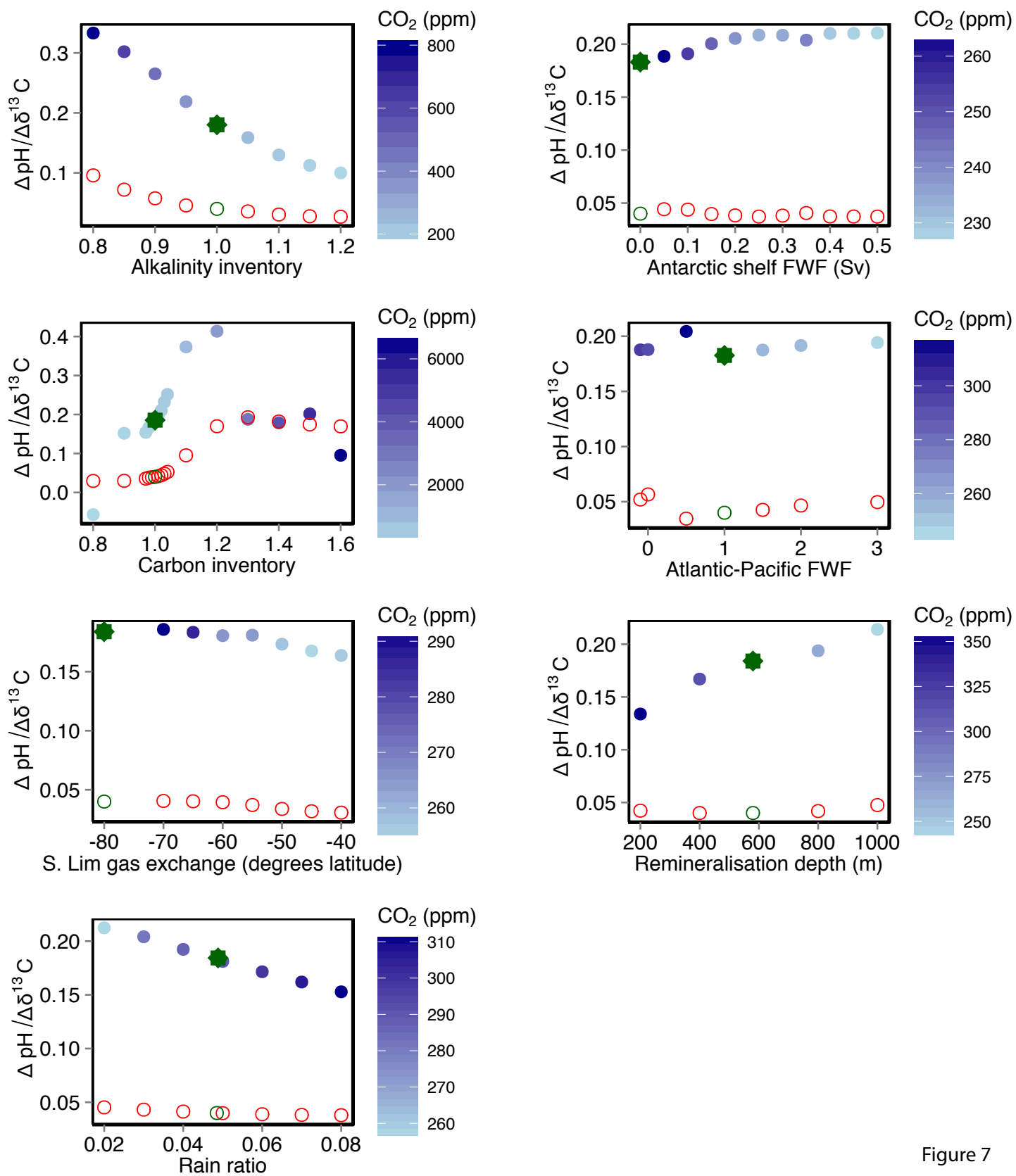


Figure 7

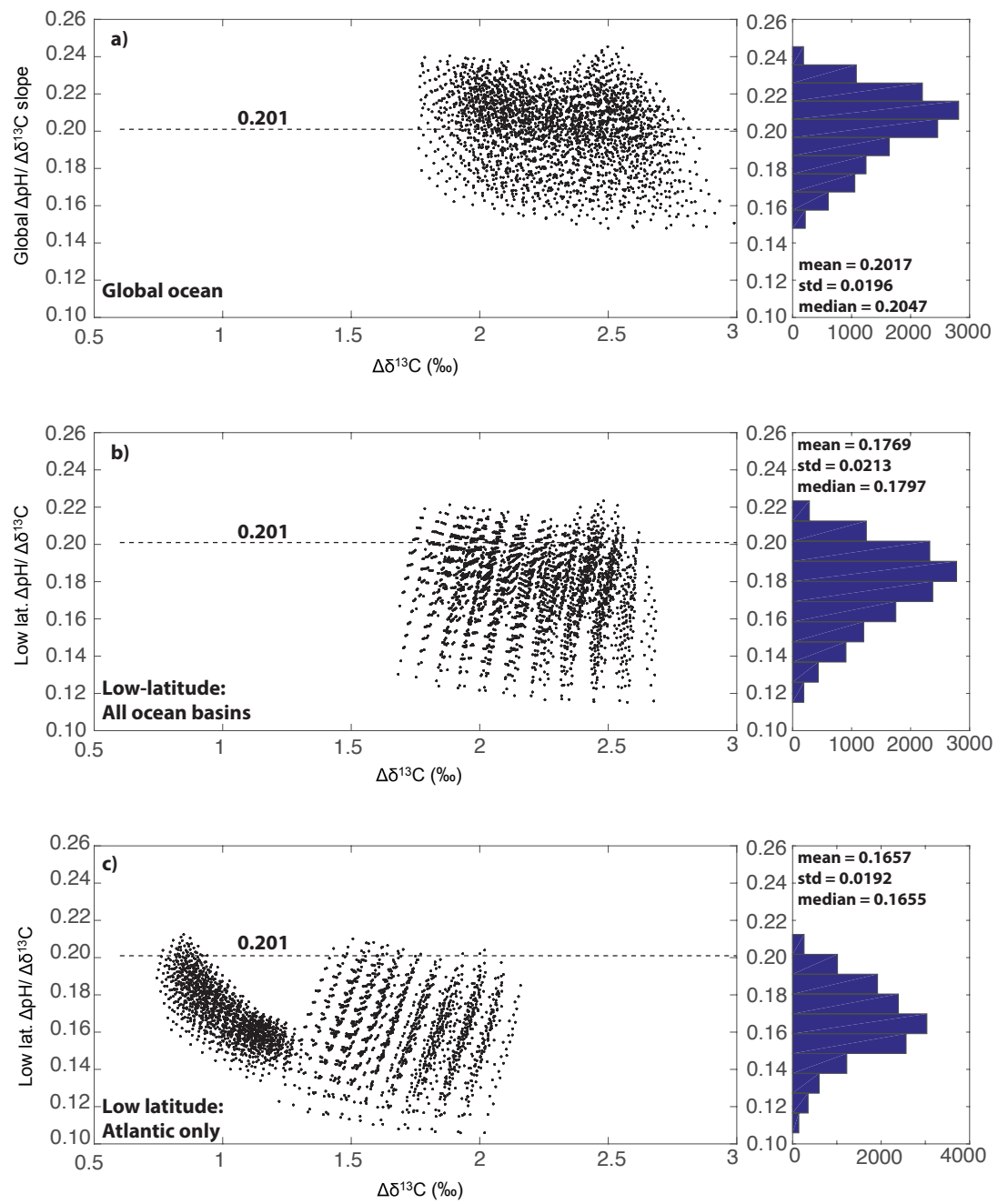


Figure 8

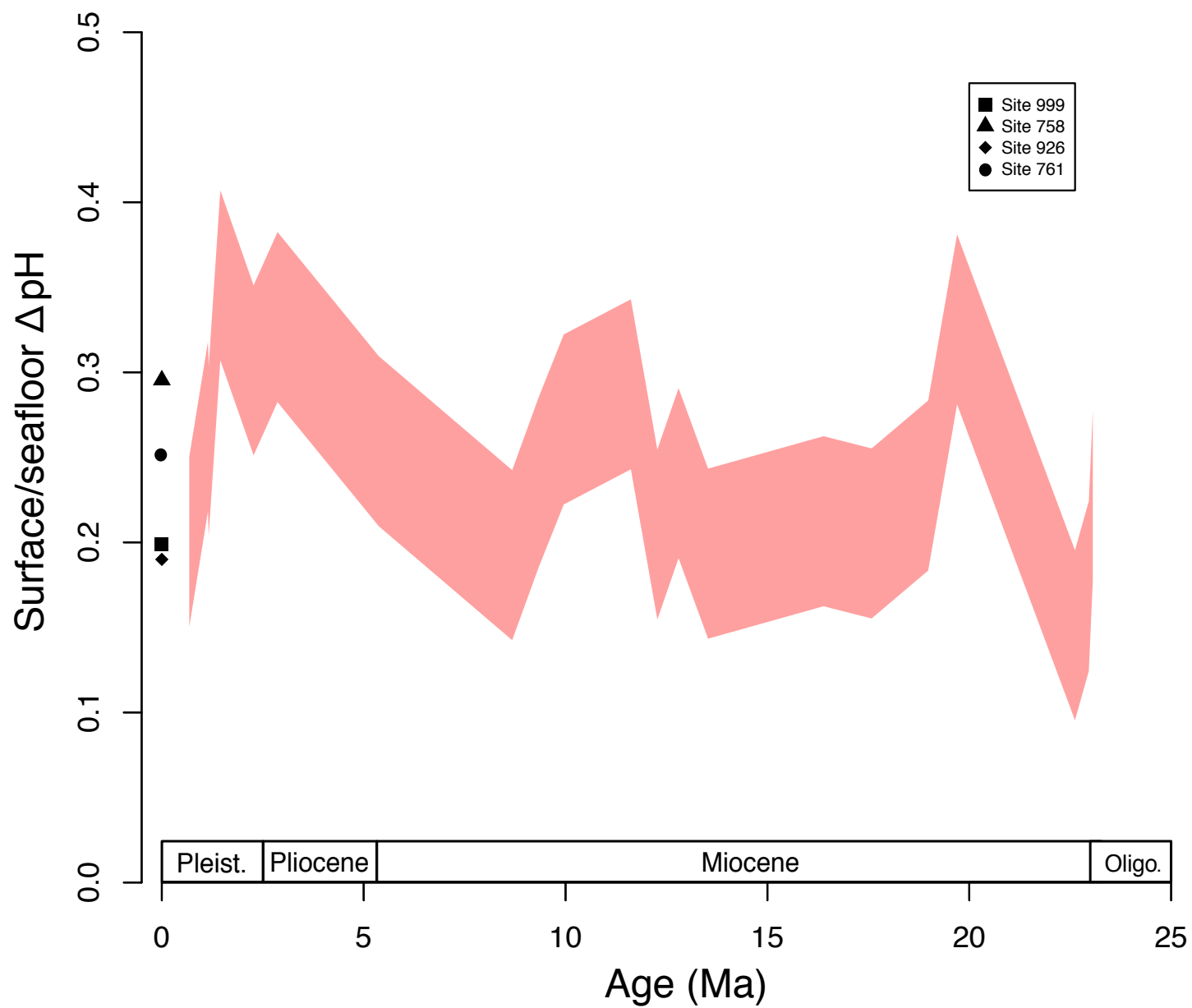


Figure 9

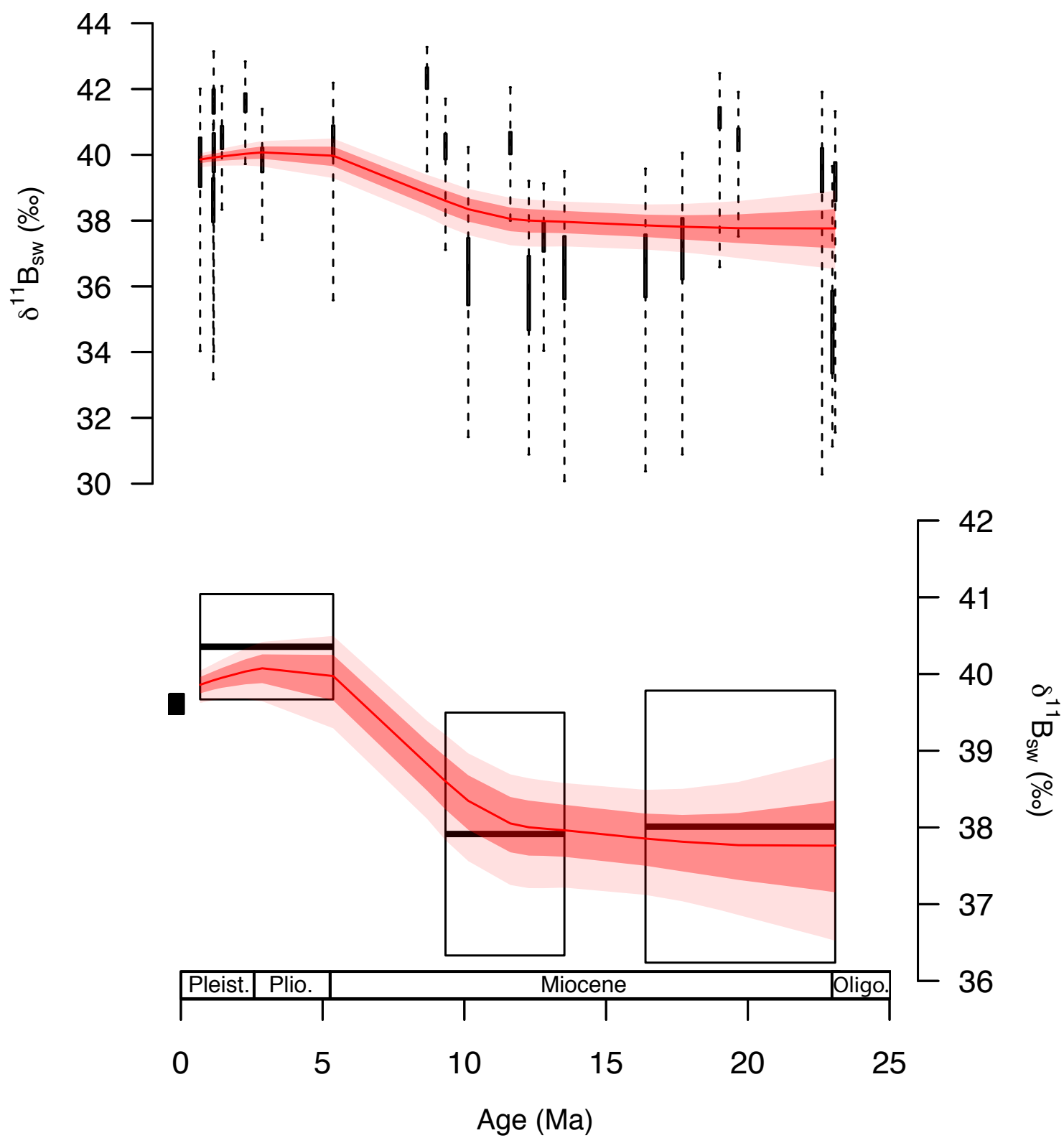


Figure 10

Figure 11

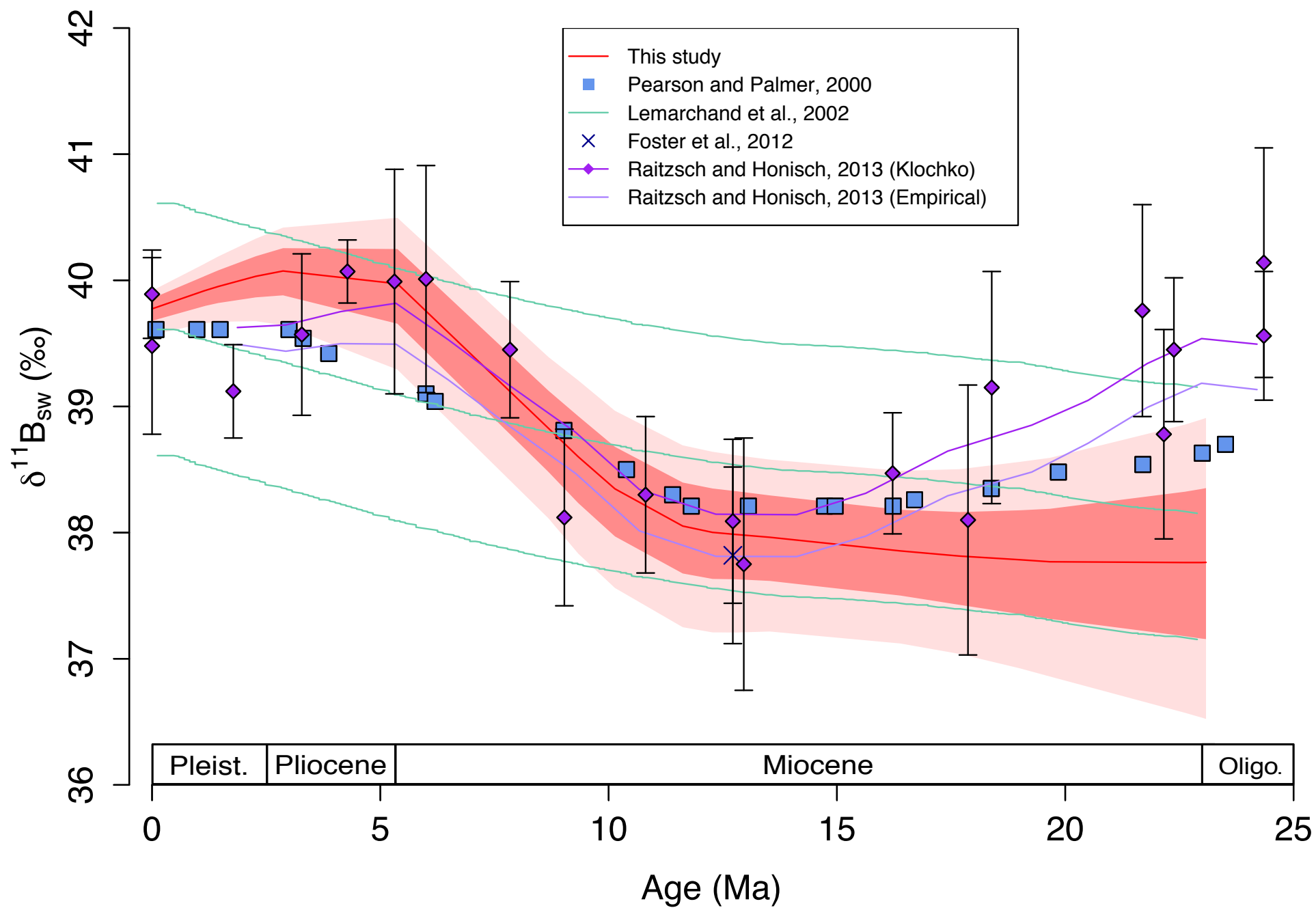
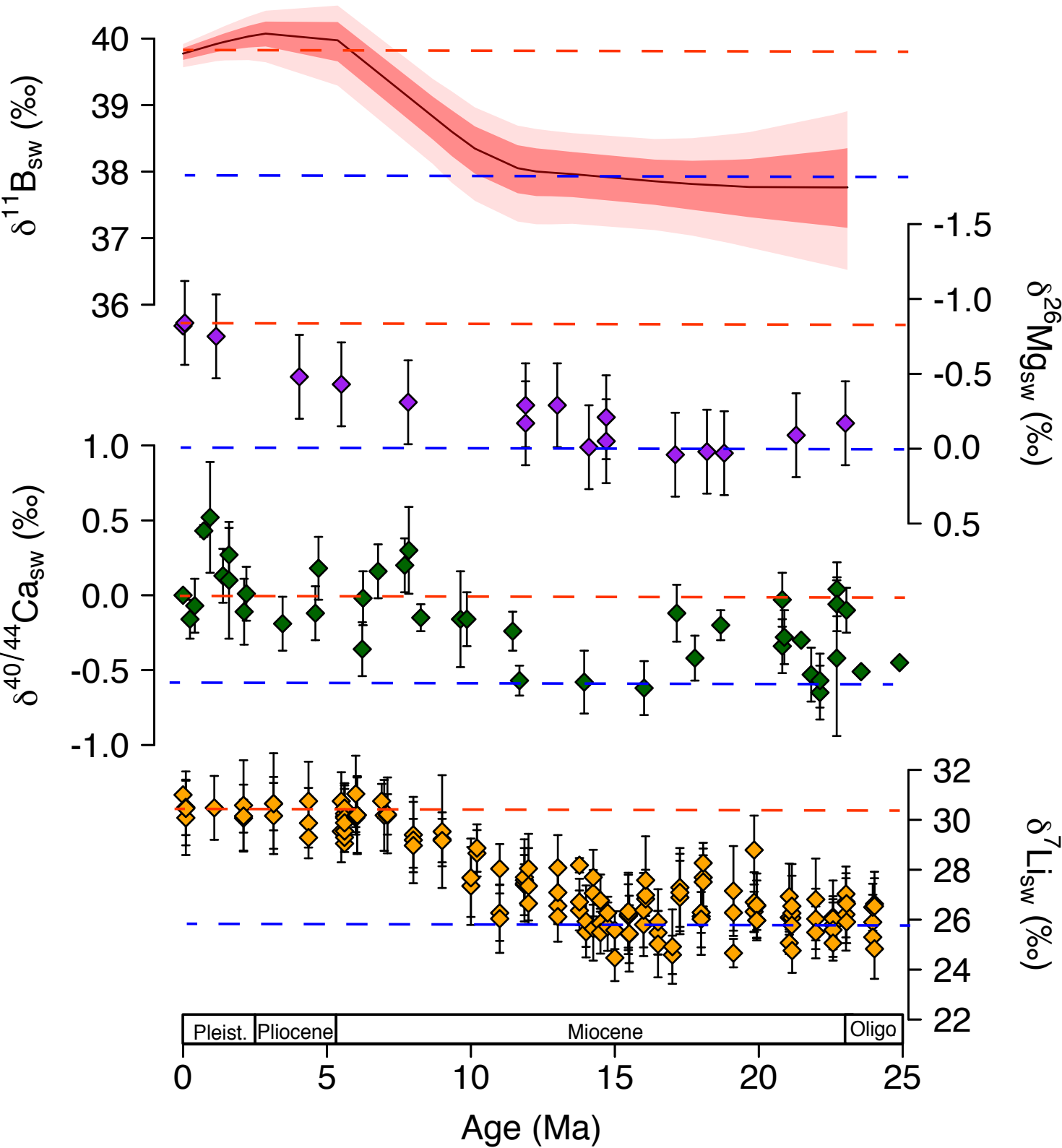


Figure 12



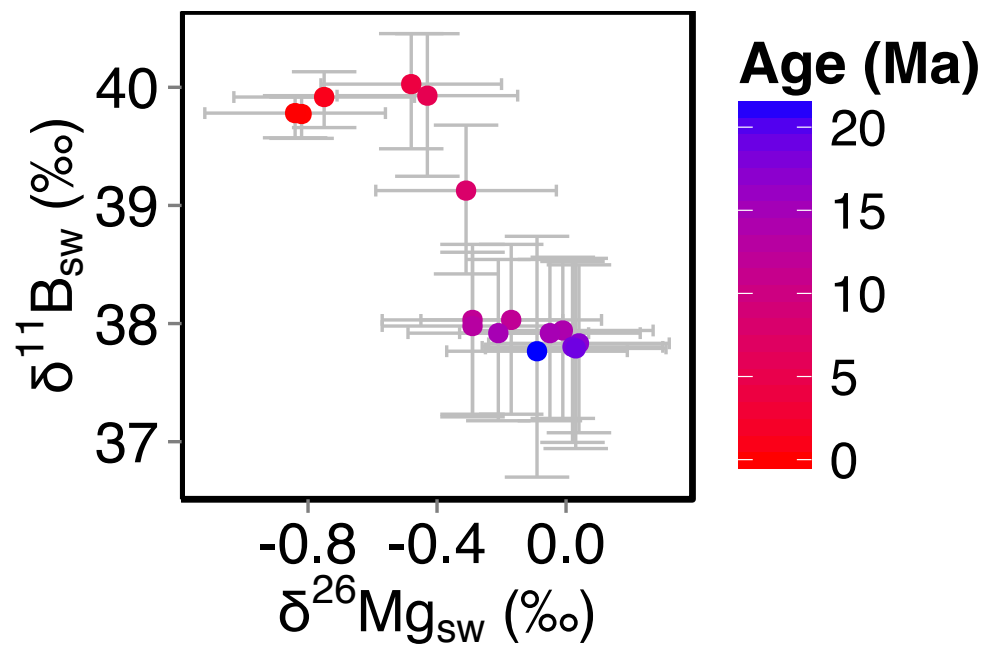
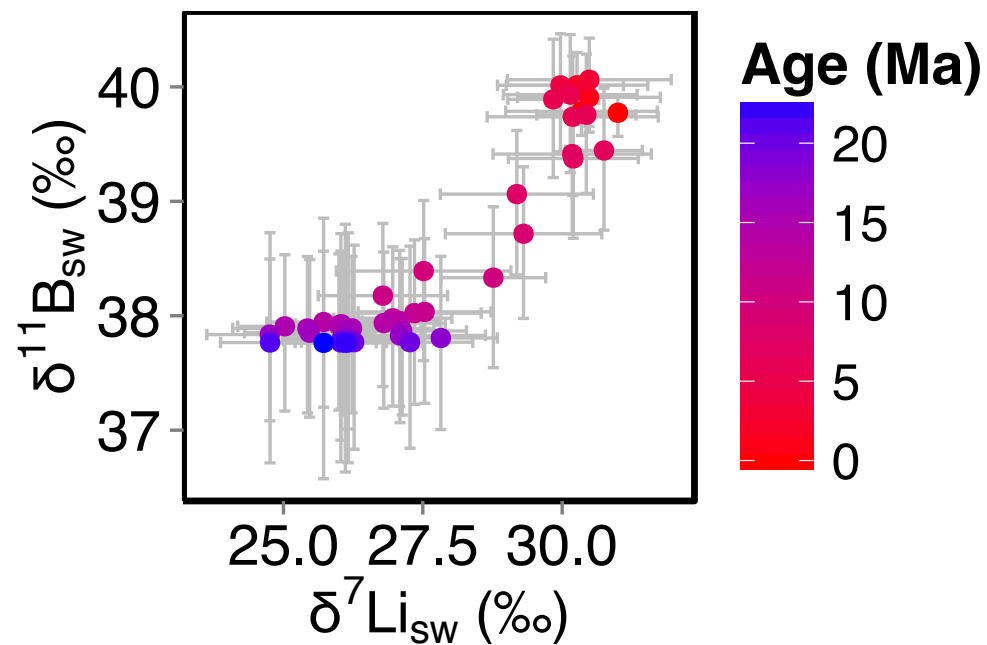
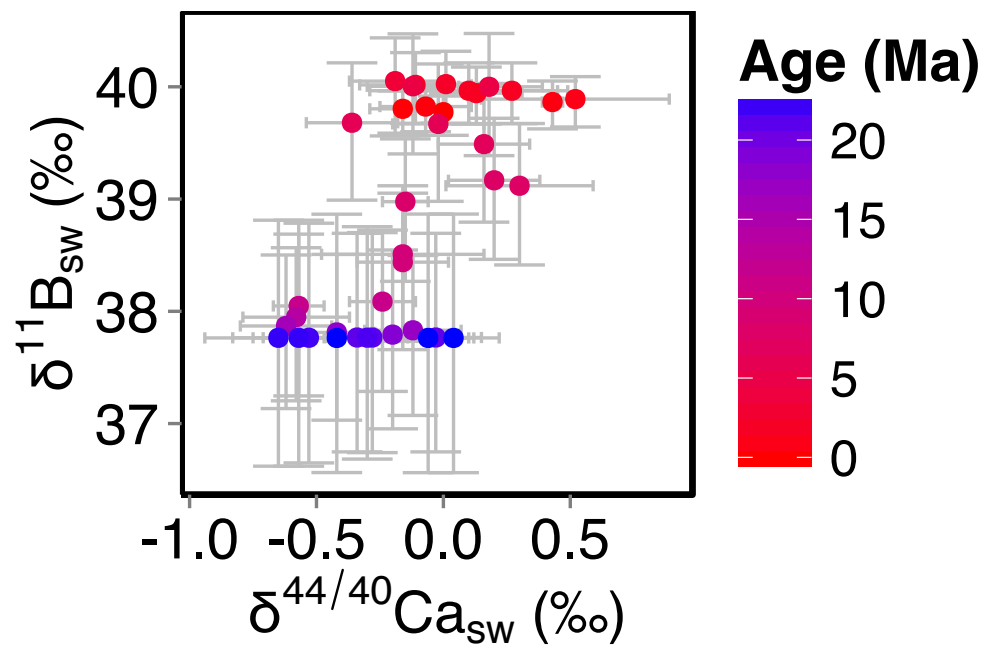


Figure 13

Table 1. CYCLOPS model parameter values defining the ensemble of 13,500 simulations*

Parameter	Description	Values assumed
PAZ surface phosphate**	unutilized polar nutrient	1μM, 1.25μM, 1.5μM, 1.75μM, 2μM
PAZ vertical exchange**	bottom water formation	2Sv, 7.75Sv, 13.5Sv, 19.25Sv, 25Sv
SAZ surface phosphate**	unutilized polar nutrient	0.7μM, 0.825μM, 0.95μM, 1.075μM, 1.2μM
AMOC circulation scheme**	deep vs. shallow overturning	NADW, GNAIW
representative timeslice***	Age ([Ca ²⁺]/CCD); calcium set outright; CCD set via riverine CaCO ₃ flux using inverse scheme	0Myr (10.6mM, 4.65km), 9Myr (12.89mM, 4.4km), 11Myr (13.33mM, 4.9km), 16Myr (14.28mM, 4.7km), 18Myr (14.57mM, 4.25km), 20Myr (14.86mM, 4.7km)
atm. CO ₂ ****	set via silicate weatherability	200ppm, 300ppm, 400ppm, 500ppm, 600ppm, 700ppm, 800ppm, 900ppm, 1000ppm

*= The six parameters assume 5, 5, 5, 2, 9 and 6 values, yielding 13,500 distinct parameter combinations

** = These parameters are intended to span the full range of ocean carbon cycling over late Pleistocene glacial-interglacial cycles, as describe in more detail in Hain et al. (2010)

*** = We selected representative timeslices based on local extrema in the CCD reconstruction of Pälike et al. (2012) and we combine these with appropriate reconstructed calcium concentrations based on Horita et al. (2002). These choices are intended to capture the range of long-term steady state conditions of the open system CaCO₃ cycle relevant to our study interval

**** = These atmospheric CO₂ levels are chosen to span a range wider than expected for the study interval. Following silicate-weathering-feedback paradigm, long-term CO₂ is fully determined by the balance of geologic CO₂ sources and silicate weathering, whereby faster acting processes of the open system CaCO₃ cycle compensate relative to that CO₂ level. All else equal, high CO₂ levels, low calcium concentrations and deep CCD correspond to high bulk ocean carbon concentrations (Hain et al., 2015) with many of the individual simulations of this ensemble exceeding 4000μM DIC.

Table 2

Input parameter	Uncertainty applied	Source of uncertainty estimate
Surface to sea floor ΔpH	Uniform +/- 0.05 pH units	Plausible range of $\Delta\text{pH}/\Delta\delta^{13}\text{C}$ in CYCLOPS and GENIE sensitivity tests; prediction error of linear $\Delta\text{pH}/\Delta\delta^{13}\text{C}$ regression in GENIE
$\delta^{11}\text{B}$ measurement	0.15-0.61‰	Long-term external reproducibility
Temperature	$\pm 2^\circ\text{C}$	Uncertainty in the Mg/Ca measurement and Mg/Ca-temperature calibration
Salinity	± 2 psu	In the absence of a salinity proxy this uncertainty is applied to cover variations through time.
Seawater [Mg]	± 4.5 mmol/kg	following Horita et al., (2002)
Seawater [Ca]	± 4.5 mmol/kg	following Horita et al., (2002)

Table 3

Sources	Isotopic Ratio			
Oceanic Inputs	$\delta^{11}\text{B}_{\text{SW}}$ 39.61 ‰	$\delta^7\text{Li}_{\text{SW}}$ 31 ‰	$\delta^{26}\text{Mg}_{\text{SW}}$ -0.83 ‰	$\delta^{44/40}\text{Ca}_{\text{SW}}$ 0 ‰
Input from hydrothermal	6.5 ^a	8.3 ^b	N/A	-0.96 ^h
Fluid from accretionary prisms	25 ^a	15 ^b	N/A	N/A
Riverine Inputs	10 ^a	23 ^b	-1.09 ^d	-1.28 ^h
Groundwater	N/A	N/A	-0.82 ^d	-1.02 ⁱ
Outputs				
Precipitation into carbonates	20 ^a	29 ^c	-3.5 ^{d,e,f}	-1.15 ^{h,j}
Ocean crust alteration	4 ^a	15 ^b	-0.83 ^{d,g}	-1.2 ^h
Absorption onto sediment	15 ^a	15 ^b	??	N/A